INTERACTIONS OF AMINO-BEARING ORGANIC ACIDS AT THE FERRIHYDRITE-WATER INTERFACE: A FLOW ADSORPTION MICROCALORIMETRY-ULTRA VIOLET VISIBLE SPECTROSCOPY STUDY

by

Marie Aurore Niyitanga Manzi

Bachelor of Science, 2020

Texas Christian University

Fort Worth, Texas

A Thesis submitted to the Graduate Faculty of the

College of Science and Engineering

Texas Christian University

in partial fulfillment of the requirements

for the degree of

Master of Science

May 2022

INTERACTIONS OF AMINO-BEARING ORGANIC ACIDS AT THE FERRIHYDRITE-WATER INTERFACE: A FLOW ADSORPTION MICROCALORIMETRY-ULTRA VIOLETVISIBLE SPECTROSCOPY STUDY

by

Marie Aurore Niyitanga Manzi

Thesis approved:

Major Professor

Richard Hanson

Ludmilla Aristilde

For the College of Science and Engineering

ACKNOWLEDGMENTS

First and foremost, I thank my parents and siblings for their continuous support, love, and prayers. They believe and encourage me every day to push my limits towards the best of opportunities life has to offer. For that and much more, I will be forever grateful and blessed. Life would not have been as exciting and enjoyable without the unconditional love and friendship of my friends: Hakeem Nsenga, Darlene Ninziza, Nasrin Farah, Deqa Yusuf, Nichole Watkins, Benite Ishimwe, Manyiel Mel, Gracia Nshimirimana, Bernadette Mendie, and Alyssa-Addie Nshimirimana. I am deeply grateful that they are part of my daily life in college because they help me push through with my professional and life goals. I will be forever indebted to my advisor, Dr. Omar Harvey, for teaching me more about science than I have ever learnt before coming to graduate school. Working besides him has shaped me into the inquisitive student and researcher that I am today and has opened doors for me to other life opportunities. Besides my advisor, I would also like to thank the rest of my thesis committee, Dr. Ludmilla Aristilde and Dr. Richard Hanson, for their insightful comments, encouragement, time and extreme patience and overall intellectual contribution to my development. Last but not least, I am grateful for my lab mates at the FROGGS lab for the collaborations, mental, and professional support they provided me with in the last two years; they made my graduate school journey much easier and enjoyable.

Table of contents

LIST OF FIGURES

LIST OF TABLES

CHAPTER 1: LITERATURE REVIEW

Introduction

Organic matter (OM)-mineral systems are ubiquitous in the environment and exhibit controlling effects on biotic and abiotic processes [1]. For instance, OM-mineral interactions have been implicated in long residence times of soil organic matter (SOM) because they stabilize organic species to mineral surfaces preventing SOM degradation by enzymes and microbes [2-4]. Additionally, soil organic carbon associated with colloidal-sized minerals has been shown to be critical to soil fertility [5, 6], disintegration of bioresistant organic contaminants has been linked to organo-mineral interactions [7], and minerals in soils and sediments can be sinks for carbon and hence potential repositories for excess atmospheric carbon [8, 9].

The OM-mineral interface in the natural environment is incredibly complex with sorption and desorption reactions involving OM in distinct phases from the mineral and the bulk solution in the environment [4, 10]. Due this complexity, there is still minimal comprehension as to how minerals and OM interact in the natural world [10] and most importantly an understanding of these reactions at an atomic level is yet to be achieved [11].

Complexity in OM and minerals

The mineral can have several types of reactive functional groups on its surfaces, varying specific surface areas, and changing electrostatic charges associated with it [4]. Aluminosilicates, amorphous aluminosilicates, and sesquioxides (oxides, hydroxides, and oxyhydroxides of Al and Fe) form the majority of sorbent surface area in soils [12]. The net surface charge of hydroxylated surfaces varies, becoming increasingly negative as pH increases while clays (smectite, illite) have a permanent negative charge arising from the substitution of ions of lower valence for ones

of higher valence within their crystal structure [12]. Dissolved organic matter can also have distinct characteristics, such as different functional groups, hydration sphere, ionic radius, valence, outer-shell electron configuration, covalent and ionic bonding characteristics, polarizability, hydrophobicity, molecular coordination, steric effects, and redox characteristics [4], all of which dictate bonding mechanisms with minerals.

Bonding mechanisms in OM-mineral systems

The abundance of OM in marine sediments has long been associated with the sorption of OM to fine-size mineral surfaces [13]. Similarly, when soils are separated by size, fine silts and clay separates contain the highest organic matter contents [14]. There is evidence that OM in terrestrial ecosystems, the largest reservoir of organic carbon [15], is preserved through physical aggregation and/or chemical sorption [10]. The major mechanisms by which OM adsorbs onto mineral surfaces have been suggested by Sposito [16] to be: 1) ligand exchange-surface complexation involving the exchange of acidic hydroxyl groups of organic matter (e.g., carboxylic and phenolic) for hydroxyl groups on the surface; 2) electrostatic interaction involving the exchange of ions between a solution and a complex or surface; 3) hydrophobic interactions where nonpolar residues are excluded from water by entropy-related interactions that force the nonpolar groups together into micelles; 4) hydrogen bonding where a hydrogen atom with a positive partial charge interacts with partially negatively charged atoms; 5) cation bridging involving the formation of positively charged bridges by polyvalent cations between the negatively charged mineral surface and the negatively charged acidic functional groups of the OM; and 6) van der Waals interactions also known as electrostatic forces caused by a temporarily fluctuating dipole moment arising from a brief shift of orbital electrons to one side of an atom or molecule, which creates a similar shift in adjacent atoms or molecules. These

mechanisms fall under a bigger umbrella of inner sphere complexation adsorption if there is direct bonding of OM to mineral surfaces and outer sphere adsorption if the OM adsorbs onto the mineral by interplay through water molecules [4].

The stability of the bonds between OM and minerals is proposed to follow a discrete zonal sequence whereby bond strength decreases with increasing distance from the surfaces [17, 18]. The contact zone between OM and the mineral is stabilized by organic-mineral associations dominated by either polar organic functional groups interacting via ligand exchange with simply coordinated mineral hydroxyls or proteinaceous materials that unfold upon adsorption [17]. A secondary hydrophobic zone contains other organic matter that maybe adsorbed into the first layer and whose components may exchange more easily with the surrounding solution [17]. An outer region or kinetic zone contains OM loosely retained by cation bridging, hydrogen bonding, and other interactions with the outer layers of the organic matter, having a more rapid turnover [17]. Desorption processes of OM have been studied to a significantly lesser extent than adsorption, with several mathematical formulations of solute transport considering the adsorption-desorption reaction reversible [19]. This has been proven to be an invalid postulation for several heavy metals interactions with several soils in batch studies [19]. The nature of the physical space at the mineral surface is another important factor that affects adsorption reactions. Minerals are often porous solids and the physical constraints of small pores create forces on water and chemicals that affect molecular interactions of the sorbed chemicals [4]. The properties of the bathing solution, such as pH, is another factor that determines minerals' surface charge and the extent of dissociation of carboxylic acids in OM and thus affecting bonding mechanisms [4]. The mineral-organic matter interface in the natural environment therefore is multidimensional and significant knowledge gaps exist regarding steric effects, distribution, and conformation of organic molecules on the surface, [20] and susceptibility of organic ligands to desorption, degradability, and exchange [19, 21].

Quantifying sorption mechanisms at the organic matter-mineral interface would provide researchers with insights into the stabilization of carbon pools.

While the type of bonding in these systems is well characterized by a variety of spectroscopic techniques, the mechanisms behind these interactions and the trends are not clear. For instance, the sorption of humic and fulvic acids on synthetic gibbsite peaked at pH 5 [22], whereas sorption on K-saturated smectite and on synthetic lepidocrocite decreased continuously over the range pH 3.2 to 7.0 [22]. In other studies with humic substances, sorption on gibbsite, montmorillonite, illite, mordenite, and amorphous silica decreased over this same pH range, whereas it decreased or stayed constant for kaolinite, and increased for δ-Al_2O_3 [23-25]. Additionally, information on controls on desorption of organics is often conflicting because several mechanisms are at work simultaneously [12].

Energetics of OM-mineral interactions

Enthalpies of adsorption measurements derived from temperature dependence of sorption isotherms in batch experiments have been traditionally used to study OM-mineral associations [26, 27]. Energy-dependent adsorption isotherms determined are based on the Clausius-Clapeyron equation, which assumes that sorption reaches equilibrium, is reversible, and leads to no change of the adsorbing surface [28]. These postulations are only acceptable when single crystal systems exhibit monolayer organic bonding onto the mineral surface for one type of binding site [29, 30]. However, minerals in the natural environment possess dynamic surfaces with a variety of sites where the reactivity and distribution change depending on crystallinity, morphology, and crystal-face orientation [11].

The direct, dynamic, highly sensitive, and quantitative nature of flow adsorption microcalorimetry (FAMC), as well as its advantages over batch systems and other calorimetric

methods, make the technique well suited for investigating changes/dynamics of complex reactions occurring at the liquid-solid interface [19, 31]. It has widely been used to study the surface chemistry of many types of solids such as organics [32, 33] and synthetic inorganics [34]. FAMC has several advantages over batch calorimetric systems: i) fine temporal resolution (seconds), ii) simultaneous monitoring of reactions occurring at different rates [19, 31], iii) easy control of physico-chemical conditions of the system (e.g. pH, ionic strength) [21], and iv) sorption and desorption processes can be performed on the same sample making it possible to determine the reversibility of the reaction [28]. Energy measured as heat is the main factor in this study because all reactions require energy or heat transfer to occur. This measured heat is also known as change in enthalpy. Coupled with Ultraviolet-visible spectroscopy (UV/vis), FAMC can yield information about how sorption energies and quantities vary with surface coverage.

The major objective of this study was to use a combined method of FAMC-UV/vis to quantify sorption dynamics, kinetics, heat of reaction, and change in surface charge of ferrihydrite associated with ferrihydrite-organics interactions. Iron is the most prevalent element in Earth's crust after oxygen, silicon, and aluminum. It circulates in biogeochemical cycles in biotic (biosphere) and abiotic (atmosphere, hydrosphere, and lithosphere) systems [6]. Under aerobic conditions, iron exists in its ferric (Fe^{3+}) form while under anaerobic conditions it exists in its ferrous (Fe^{2+}) form . Ferrous iron is soluble while ferric iron is insoluble [6]. Consequently, the ferric form is the predominant form found in naturally occurring, iron-bearing minerals, like the iron oxyhydroxide used in this study [6]. Organic acids used in this study were amino-bearing carboxylic acids (glycine, α-alanine, β-alanine, G3.5-COOH) and ATP. These were chosen to reflect differences in size, molecular conformation, and deprotonation behaviors. Additionally, these molecules are environmentally and/or technologically significant. Glycine and α-alanine, typically chosen as good models for studying biological systems exhibiting peptide bonds, are

the simplest proteinogenic amino acids used as food additives and precursors for chemical and pharmaceutical products [35]. β-alanine is a non-proteinogenic amino acid incorporated in Vitamin B5 and is employed in secondary metabolism in plants (lignin biosynthesis) [36]. Amino acids are characterized by two active functional groups, the amine and carboxylic groups (NHx and COO (H)), which define the chemical form of the molecules and can be involved in bonds formed with ferrihydrite. Depending on the pH environment, the chemical speciation of glycine, α-alanine, and β-alanine in solution vary from cationic ($NH_3^+CHRCOOH$) through zwitterionic to anionic $NH_2CHRCOO^-$) forms (see appendix).

The poly amido amine (PAMAM) dendrimer G3.5-COOH was chosen for this study as a model for operationally dissolved (< 0.45 μm) larger synthetic amino-bearing organic compounds. Made of repeating units of amine and amide groups branching out into -COOH groups, the G3.5-COOH dendrimer also exists as a cation, zwitterion, or anion depending on the pH of the environment. Lastly, adenosine triphosphate disodium (ATP) completes the list of amino-bearing organic acids chosen for this study. ATP is a ubiquitous nucleotide that acts as a reservoir and energy conveyer in terrestrial and marine photosynthetic processes[37]. ATP consists of an adenine base bound to a ribose molecule, which is bound to a tri-phosphate unit at the fifth position of the ribose. Depending on the pH of the environment, the terminal phosphate and nitrogen of the base (N-7) dictate the dominant species and sorption behavior of ATP. ATP's phosphate groups will allow comparisons to be drawn between nitrogenous based organic carboxylates and phosphates to understand how the energy dynamics at the organic-ferrihydrite interface is affected by the type of organic acid involved. A notable mechanism expected in particular is the ferrihydrite-enhanced dephosphorylation of ATP leading to inorganic phosphate [37] adsorption on the mineral surface and preventing Pi release into solution, and the production of

other ribonucleotides (AXPs), namely adenosine monophosphate [38] and adenosine diphosphate (ADP) [39].

This study was accomplished through several specific tasks. Task 1 was to extract energy-based and quantity-based sorptive information from interactions between different classes of amino-bearing organic acids (glycine, α-alanine, and G3.5-COOH) and ferrihydrite at pH 5. Task 2 was to monitor interactions between β-alanine (amine group is in-plane with the carboxyl group and is attached to the β-carbon) and α-alanine (amine group is out of plane with the carboxyl group and is attached to the α-carbon) with ferrihydrite at pH 5 to quantify the effect of the position of the amine group relative to the carboxyl group on sorption dynamics, kinetics, heat of reaction (ΔH in kJ/mol), and surface charge of ferrihydrite. Task 3 was to use non-hydrolyzable G3.5-COOH and hydrolyzable ATP as amino-bearing organic acids of interest in order to study their interactions with ferrihydrite at pH 5 to compare the effect of hydrolizability and/or the lack of it on sorption dynamics, kinetics, heat of reaction (ΔH in kJ/mol), and surface charge of ferrihydrite. The G3.5-COOH and ATP have pK_{a1} at 4.5 and 4.3 and pK_{a2} at 6.3 and 6.5 respectively.

CHAPTER 2: EXTRACTING INFORMATION ON SORPTION CHARACTERISTICS FROM FAMC-UV/VIS

Introduction

The controlling effects of organic matter (OM)-mineral interactions and the trajectory of a system are inextricably linked to the nature and dynamics of sorption between the organic sorbate and the mineral sorbent [40]. The types of bonding in these systems have been identified and well characterized by a variety of spectroscopic techniques and range from weak van der Waal's forces, hydrogen bonding, cation bridging, hydrophobic interactions, to ion exchange and permanent ligand exchange [41]. Due to the complexity in OM-mineral interactions however, significant knowledge gaps exist regarding steric effects, distribution, and conformation of organic molecules on the surface [42] and susceptibility of organic ligands to desorption, degradability, and exchange [43-45].

Electrostatic interactions and reversible sorption were identified as the dominant mechanisms for simple ion exchange between NO_3^- and Cl^- in an Al(III)-substituted Fe(III) hydr(oxide) system [31]. Similar mechanisms were observed for exchange reactions between Na^+ and K^+ on amorphous aluminum hydroxide [46]. Unlike the behavior of simple ions, conflicting reports on OM-mineral associations exist due to the complexity in the organic and mineral phases [22-25]. For instance, the sorption of humic acid on synthetic gibbsite was found to peak at pH 5 in one study [22] and to decrease continuously over a pH range of 3.2 to 7.0 in other studies involving gibbsite, montmorillonite, illite, mordenite, and amorphous silica [23-25].

The objective of this study was to use combined Flow adsorption microcalorimetry-Ultraviolet visible spectroscopy (FAMC-UV/vis) to extract key sorptive properties of different classes of amino-bearing organic acids at the ferrihydrite-water interface. FAMC in conjunction

with the UV/vis together provide measurements of the energy and quantity respectively involved in reactions. Since all reactions require energy/heat transfer to occur, it follows that for simple reactions the quantity and energy should be directly proportional as shown by the equation below:

$$E_{total} = K\, Q_{total} \qquad [2\text{-}1]$$

where E_{total} represents the total energy (kJ g^{-1}) involved in the reaction, Q_{total} is the total quantity (mol g^{-1}) transferred from one medium to the other during the reaction, and K is a constant which gives the molar heat of reaction (kJ mol^{-1}). Evaluation of the relationship between energy and quantity of solutes involved in the reaction provides mechanistic insights into changes occurring along the spectrum of bonding. Here, the objective was to use FAMC-UV-vis to extract information on sorption dynamics, kinetics, heat of reaction, and change in surface charge of ferrihydrite from interactions of different classes of amino-bearing organic acids with ferrihydrite at pH 5.

Materials and Methods

Synthesis and characterization of ferrihydrite

Ferrihydrite was synthesized using a modified method by Villacís-García [47]. A solution of 7.5 g of $Fe(NO_3)_3{\cdot}9H_2O$ in 200 ml of deionized water was adjusted to a pH of 7.5 by the drop-wise addition of 1M NaOH in a 500 ml conical flask at room temperature. The resulting suspension was repeatedly washed in nanopure water and centrifuged until electrical conductivity of the suspension was <80µS cm^{-1} which is indicative of removal of sodium nitrate ($NaNO_3$) salts. The resulting paste was then dried at 80 °C overnight, crushed in an agate mortar and pestle and sieved to particle sizes of < 125 µm and 125-250 µm. The resulting < 125 µm

powders were used in x-ray diffraction (XRD) and thermogravimetric (TGA) analyses, while 125-250 μm powders were used in other subsequent characterization and all adsorption/desorption experiments.

Morphology, crystallinity, and thermal degradation characteristics of ferrihydrite were investigated using scanning electron microscope [48], x-ray diffraction (XRD) and thermogravimetric (TGA) techniques, respectively. For SEM analysis, the oxide powders were mounted using conductive carbon tape onto 10 mm metal mounts and then sputter coated with gold and imaged at 10 kV. All imaging was done on a JEOL JSM-7100F scanning electron microscope. For XRD analysis, samples were mounted as randomly oriented powders on a 0.2 mm deep dry powder plate and analyzed from 2-theta 15 to 80 degrees (2.5° min^{-1}) on a Rigaku SmartLab SE Multipurpose X-ray diffraction system, equipped with a Cuκα x-ray source and running at a voltage of 40 keV and 30 mA [49]. Thermogravimetric analysis (TGA) was performed using between 10 and 15 mg of sample under air flow of 100 mL/minute, temperature ramp of 10°C/minute between a temperature range of 30°C to 500 °C. TGA analysis was performed on a TA Q600 SDT simultaneous DSC/TGA calorimeter [50]. Details on the properties of the ferrihydrite applies to all chapters and are covered in greater details in the appendix.

Amino-bearing organic acids

The amino-bearing organic acid solutions used were glycine, α-alanine, and polyamidoamine dendrimer generation 3.5 (G3.5-COOH) at pH 5. Some physicochemical properties that would influence their sorption properties are summarized in Table 2-1. Concentrations of glycine, α-alanine, and G3.5-COOH were such that $[COOH]_{total}$ = 18.1mM. That is, [glycine] = 18.1mM, [α-alanine] = 18.1 mM, and [G3.5-COOH] = 2.8×10^{-2} mM. Note that the G3.5-COOH was set to 64 times lower concentration to account for its 64 total COOH

groups. All three molecules were dominantly in their zwitterionic form as indicated by molecular electrostatic potential (MEP) in Fig 2-1.

Table 2 - 1 . Selected physicochemical properties for glycine, α-alanine, and G3.5-COOH interacting with ferrihydrite at pH 5

Amino-based organic acid	Molecular weight (g/mol)	pK_{a1}	pK_{a2}	Speciation at pH 5 (%)			Length (nm)	Width (nm)
				Cationic	Zwitterionic	Anionic		
glycine	75.1	2.34	9.6	0	100	0	0.5	0.25
α-alanine	89.1	2.34	9.69	0	100	0	0.5	0.35
G3.5-COOH	12931	4.5	6.3	24	76	4		3.5-4.5

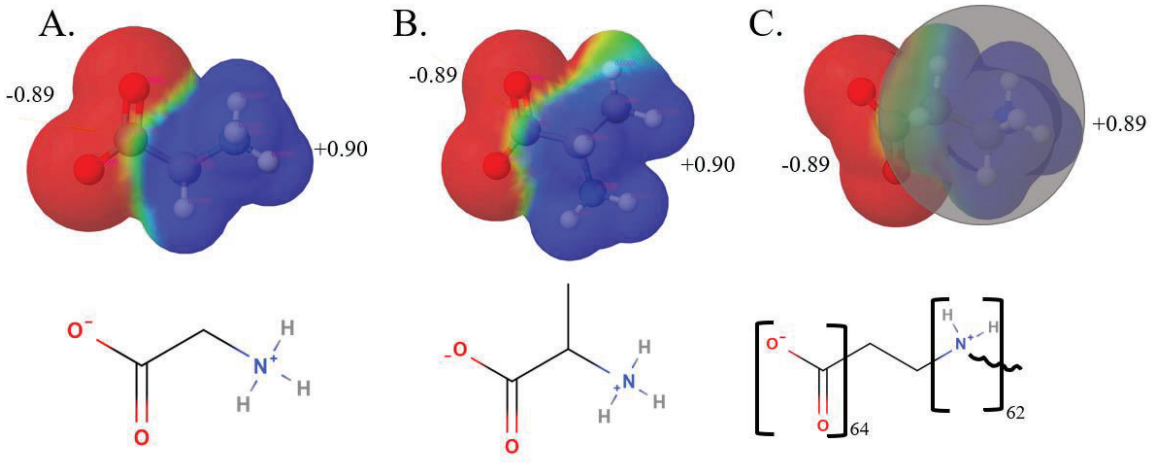

Figure 2-1: Distribution of molecular electrostatic potential (MEP) at pH 5 around (A) glycine, (B) α-alanine, (C) Poly amido amine (PAMAM) dendrimer G3.5-COOH's 64 terminal carboxyl groups and 62 tertiary amine groups (in the branches of the dendrimeric molecule). Molecular simulations were generated in MolView.

Flow adsorption microcalorimetry-Ultraviolet-visible spectroscopy (FAMC-UV/vis)

The flow calorimeter used was designed and built by Dr. Harvey. The central part of the calorimeter is the sensing unit shown in Figure 2-2. The unit is equipped with a glass microcolumn which holds a maximum of 300 mg of ferrihydrite, two NTC-type thermistors (with a negative temperature coefficient) that form one-half of an electronic bridge, and a calibrating resistor that facilitates conversion of voltage response to energy. Thermistor 1, the reference thermistor, senses the initial temperature of the reacting solution as it enters the unit. Thermistor 2, the column thermistor, senses the temperature of the effluent as it leaves the microcolumn, after the solute-sorbent reaction has occurred. A change in solution temperature due to solute-sorbent interaction produces a differential voltage between reference and column thermistors. This calorimetric response is amplified and recorded as a thermogram of voltage versus time in 1-5 second intervals until thermal equilibrium is achieved.

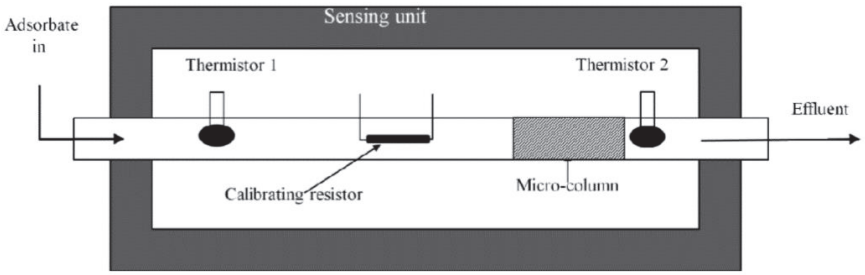

Figure 2-2: Basic design and outlay of the sensing unit for the flow microcalorimeter showing relative positions of the reference thermistor (Thermistor 1), the column thermistor (Thermistor 2), microcolumn for the sorbent and the calibrating resistor.

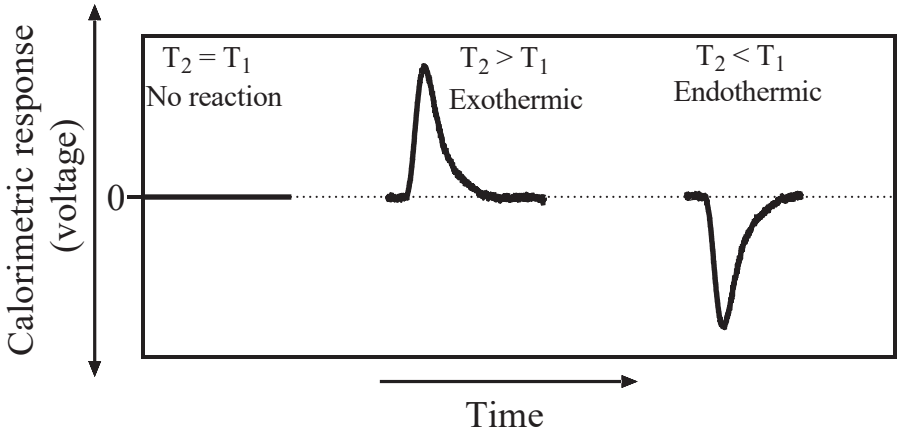

Figure 2-3: Heat signals/thermograms produced as a result of differences between temperatures detected at thermistor 2 (T2) and thermistor 1 (T1) of the sensing unit.

No detected temperature difference between Thermistor 2 and Thermistor 1 ($T_2 = T_1$) is indicative of thermal equilibrium arising from no (or no further) reaction between the solute in the solution and the sorbent in the glass microcolumn. A positive deviation ($T_2 > T_1$) is indicative of heat being added to the system as a result of an exothermic solute-sorbent reaction while a negative deviation ($T_2 > T_1$) is indicative the solute-sorbent reaction being endothermic and hence removing heat energy from the system (Fig. 2-3). An exothermic or endothermic reaction is complete with return to baseline/thermal equilibrium.

Here, thermal equilibrium within the microcolumn was achieved by flowing a background electrolyte of $NaNO_3$ (10 mM; pH 5) at a flow rate 0.5 ml min^{-1} through the microcolumn (containing 50 ± 0.5 mg of ferrihydrite) until a baseline/thermal equilibrium is achieved. Baseline/thermal equilibrium was indicative of 1) the elimination of heats of wetting in ferrihydrite and 2) saturation of positive charge sites on ferrihydrite with NO_3^-.

Once thermal equilibrium and a NO_3^- saturated ferrihydrite was achieved the following experimental protocol was used: Pre-probe anion exchange characteristics were assessed using alternating cycles of Cl^- replacing NO_3^- (Cl^-/NO_3^-) and NO_3^- replacing Cl^- (NO_3^-/Cl^-) (Fig. 2-4). This was achieved via a switching valve where the valve position was set to allow NaCl (10 mM; pH 5) to flow through the micro column to initiate Cl^- for NO_3^- exchange. Once Cl^- for NO_3^- anion exchange was completed as evidenced by a return to baseline, the valve was switched to flow $NaNO_3$ (10mM; pH 5) through the micro column. This facilitated NO_3^- for Cl^- exchange on the Cl^- saturated ferrihydrite. A total of two pre-probe Cl^-/NO_3^- and NO_3^-/Cl^- cycles were collected on each sample prior to the examination of organic probe-ferrihydrite interactions. The last cycle was always a NO_3^-/Cl^- cycle to return the surface to NO_3^-- saturated ferrihydrite status.

Organic sorption and desorption from ferrihydrite were assessed (Fig. 2-4). The switching valve was set to allow the organic solution to flow through the micro column containing the NO_3^-- saturated ferrihydrite. After the sorption reaction was completed, the valve was set to allow NO_3^- solution ($NaNO_3^-$) to flow through the now organic probe-saturated ferrihydrite. This represented the "desorption" cycle of the experiment. In both the sorption and desorption cycle absorbance of effluent was continuously monitored on the UV/vis at a wavelength that was shown to produce a standard curve that obeys Beer's law up to concentrations used in this study (see appendix).

Post-probe anion exchange characteristics were performed on the NO_3^-- saturated ferrihydrite following the desorption stage (Fig. 2-4). Once the desorption stage was completed, as evidenced by a return to baseline, the valve was switched to flow NaCl through the micro column to facilitate Cl^-/NO_3^- exchange. Once Cl^- for NO_3^- anion exchange was completed as evidenced by a return to baseline, the valve was switched to flow $NaNO_3$ through the micro column. This facilitated NO_3^- for Cl^- exchange on the Cl^- -saturated ferrihydrite. A total of two post-probe Cl^-/NO_3^- and NO_3^-/Cl^- cycles were collected on each sample after the desorption of the organic probe from ferrihydrite.

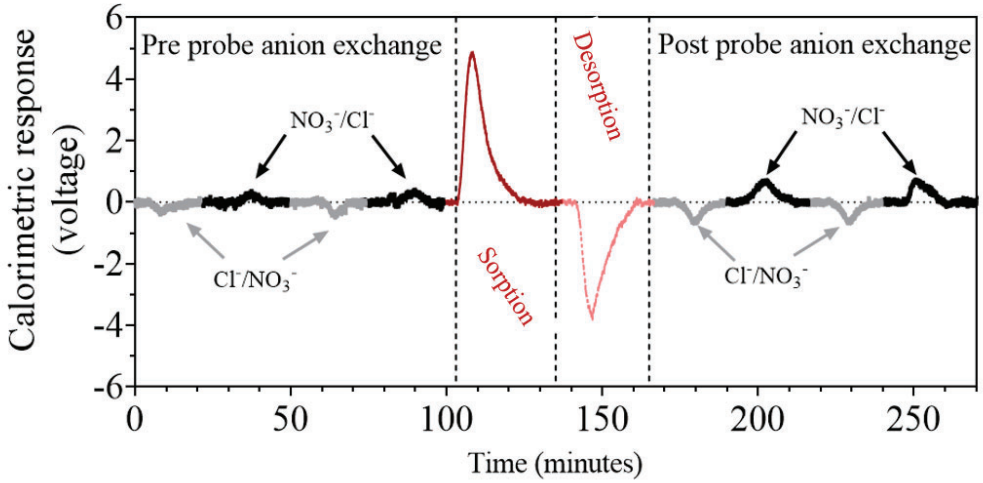

Figure 2-4: Displayed signal (volts) over time (minutes) for flow adsorption microcalorimetry (FAMC) running protocols. Left to right: pre-probe anion exchange, sorption, desorption, post-probe anion exchange. Glycine is the probe interacting with ferrihydrite at pH 5 in this figure.

Data handling and analysis

Dynamics, kinetics, and energetics of amino-bearing organic acid interactions with ferrihydrite were assessed via a series of systematic analyses involving raw differential voltage versus time thermograms, their integration and transformation to weight-adjusted energy (E_i; J/g), the side-by-side energy analyses and deconvolution of E_i and cumulative sorption (Q_{sorb}; mmol/g) or desorption (Q_{des}) curves from UV/vis spectroscopy, and the association of overall and deconvoluted E_i, $Q_{sorp,}$ and Q_{desorp} curves. Details on how integration, deconvolution, and association of E_i, $Q_{sorp,}$ and Q_{desorp} were executed is provided in the appendix.

Raw differential thermograms versus time allowed for the assessment of reaction time, whether the reactions were exothermic, endothermic, or mixed, and comparative magnitudes of energy change. Weight-adjusted energy (E_i; J/g), Q_{sorp}, and Q_{desorp} were used to assess the overall reaction dynamics (energy, sorption, desorption), total reaction energy (E_{total}), total quantity sorbed (Q_{sorp}) and total quantity desorbed (Q_{desorp}). Deconvolution of E_i, Q_{sorp}, and Q_{desorp} was used to assess the number of reaction steps, their respective contribution to the total reaction, and respective rate constants. Here logistic equations of the following form were used:

$$E_i = [\frac{E_{total}}{(1 + 10^{k'(t-t_{1/2})})} + \cdots]_n \qquad [2-2]$$

$$Q_i = [\frac{Q_{total}}{(1 + 10^{k'(t-t_{1/2})})} + \cdots]_n \qquad [2-3]$$

where, E_i is the measured differential energy at time t; E_{total} is the differential energy when the reaction goes back to baseline; k' is the rate constant of the reaction; $t_{1/2}$ is the time when 50% of the reaction is complete; n is the number of reaction steps. Q_i is the measured cumulative quantity at time, t; Q_{total} is the cumulative quantity when the reaction goes back to baseline; k' is

the rate constant of the reaction; $t_{1/2}$ is the time when 50% of the reaction is complete; and n is the number of reaction steps. The optimized number of reaction steps was determined via error minimization between experimental data and equations 2-2 and 2-3 (see appendix).

In assessing the effects of the amino-bearing probes on ferrihydrite anion exchange characteristics, pre-probe NO_3^-/Cl^- and Cl^-/NO_3^- behavior was compared to that of post-probe NO_3^-/Cl^- and Cl^-/NO_3^- behavior. Specifically, E_{total} (J/g) given by peak area/integral of power curves were compared to quantify the difference between post- and pre-probe anion exchange (J/g) energy on the surface. This allowed for the assessment of whether sorption followed by desorption of the probe on the surface increased, decreased or had no effect on E_{total} for anion exchange on the surface.

Results and Discussion

Sorption and desorption dynamics and kinetics

Raw calorimetric response thermograms for glycine, α-alanine, and G3.5-COOH onto NO_3^- saturated ferrihydrite at pH 5 are shown in Fig. 2-5 A. Thermograms for the reverse reaction (i.e. NO_3^- sorption to glycine, α-alanine, and G3.5-COOH-saturated ferrihydrite) are shown in Fig. 2-5 B. In all cases, thermograms for sorption and desorption of the amino-bearing organic acids were log-normal in shape with reaction time lasting between 15-20 minutes (Fig. 2-5). The log-normal shape in the thermograms was consistent with an initial fast phase sorption followed by a slower (more diffusive) sorption/desorption reaction (Fig. 2-5). Reaction times of 15-20 minutes were shorter than reported from previous studies of ligand exchange on metal hydr(oxides)[31] but consistent with reports for simple ion exchange reactions[51]. A recent study by Leonce et. al [52] on (hydroxy)cinnamates interactions with ferrihydrite also showed that the involvement of van-der Waals in OM-mineral associations cannot be ruled out.

Differential voltage thermograms pointed to glycine and α-alanine sorption to NO_3^--saturated ferrihydrite occurring via purely exothermic reaction steps (Fig. 2-5). In contrast, sorption of G3.5-COOH to NO_3^--saturated ferrihydrite was mixed with the first half being exothermic and the other half being endothermic (Fig. 2-5). Given the spontaneous nature of the reactions at the experimental temperature (22 ± 2.5ºC) and the requirement of spontaneous reactions having $-\Delta G$ (where $\Delta G = \Delta H - T\Delta S$), it is reasonable to postulate that for glycine and α-alanine with exothermic sorption steps, that carry a $-\Delta H$ value by convention, their sorption to NO_3^--saturated ferrihydrite required no increase in entropy (ΔS)/disorder of the system to facilitate sorption. By contrast, the spontaneous sorption observed for G3.5-COOH with its endothermic sorption ($+\Delta H$) would require an increase in entropy/disorder of the system. The endothermic nature of NO_3^- interacting with glycine, α-alanine, and G3.5-COOH-saturated ferrihydrite indicated that spontaneous desorption of amino-bearing organic acids from ferrihydrite by NO_3^- at pH 5 required increased entropy. That is, while the sorption for glycine and α-alanine to NO_3^--saturated ferrihydrite is enthalpy-driven, that for G3.5-COOH and the desorption of all three molecules from ferrihydrite by NO_3^- is entropy-driven at pH 5 and room temperature. Increased entropy that would drive spontaneous sorption/desorption reactions in aqueous systems is often attributed to rearrangement of water at the surface-water interface and/or hydration sphere of the sorbate in water. For instance, it is well accepted that the water molecules at the surface of nanocrystalline oxides like ferrihydrite are highly disordered compared to more crystalline counterparts like hematite or goethite[53]. G3.5-COOH and similar dendrimeric amino-bearing organic acids are known to change molecular conformation in reaction environments[54]. Such molecular conformational change around the molecule and the ferrihydrite surface could plausibly account for increased entropy for a spontaneous reaction.

Cumulative energy curves were qualitatively consistent with entropy-driven sorption following the order G3.5-COOH > α-alanine > glycine with E_{total} values of 0.16 J/g, -1.52 J/g, and -3.13 J/g respectively (Fig. 2-6 A). By contrast entropy-driven desorption (Fig. 2-6 B) followed the order glycine (+2.59 J/g) > α-alanine (+1.42 J/g) > G3.5-COOH (+1.35 J/g). Deconvolution of energy curves was in agreement with sorption of glycine, α-alanine, and G3.5-COOH onto ferrihydrite occurring in two distinct reaction steps (Fig. 2-7). Subsequent desorption of glycine and α-alanine by NO_3^- also followed two reaction steps but the desorption of G3.5-COOH occurred in one reaction step (Fig. 2-7). Fitted rate constants, *k'*, pointed to glycine and α-alanine being desorbed at similar rates but 1.5-2 times slower than G3.5-COOH (Table 2-2). For a given amino-bearing organic acid, the first sorption step occurred at 1.5-2.2 times faster than the slower second sorption step (Table 2-2). Desorption generally occurred at slower rates than sorption with desorption rates being similar across reaction steps and amino-bearing organic acids (Table 2-2). Deconvolution of Q_{sorb} and Q_{des} curves yielded very comparable trends, and absolute values in rate constants for both sorption and desorption reactions across glycine, α-alanine, and G3.5-COOH (Fig. 2-8). This was consistent with the same kinetic information being contained in energy- and mass-based data from FAMC and UV-vis, respectively (Fig. 2-9).

Comparison of deconvoluted E_i, Q_{sorp}, and Q_{desorp} curves further pointed to glycine and G3.5-COOH sorption to NO_3^--saturated ferrihydrite being completely reversible by NO_3^- (Fig 2-7; Fig 2-8). However, α-alanine sorption was only partially (≈ 10%) reversible by NO_3^-. Q_{sorp} peaks also showed that while removal of glycine and G3.5-COOH achieved equilibrium in all reaction steps, for α-alanine equilibrium was achieved in reaction step 1 but not reaction step 2 (Fig 2-8). It is worth noting that such non-equilibrium removal of α-alanine from solution has

been observed previously and attributed to intra-aggregation of α-alanine with a soil allophane [55] and crystal deposition of α-alanine on alumina by hydrogen bonding [56].

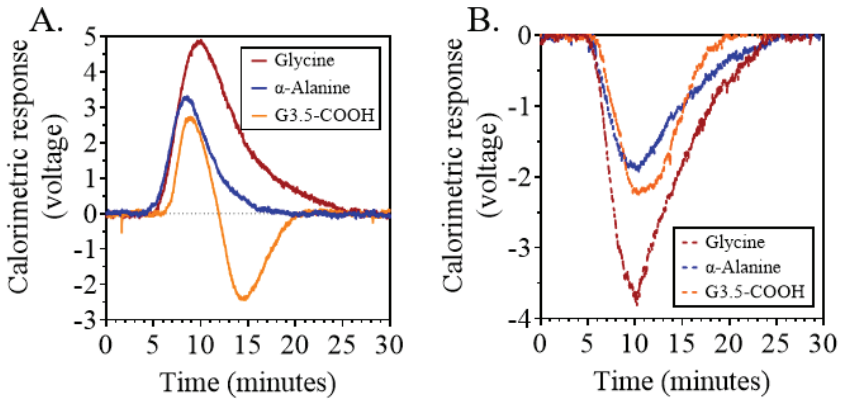

Figure 2-5: Calorimetric signals in voltage for (A) amino-bearing organic acids/probe interacting with a nitrate (NO_3^-) saturated ferrihydrite and (B) NO_3^- interacting with a probe saturated ferrihydrite.

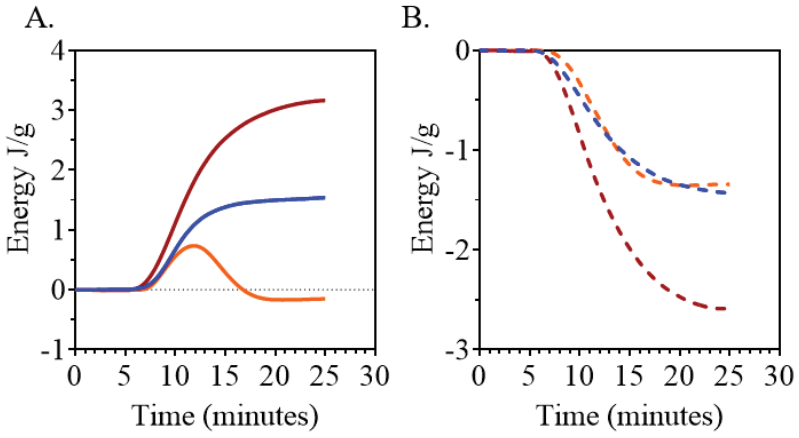

Figure 2-6: Integrated energy peaks (J g^{-1}) for sorption (probe/NO_3^-) and desorption (NO_3^-/probe) of red: glycine, blue: α-alanine, orange: PAMAM G3.5-COOH.

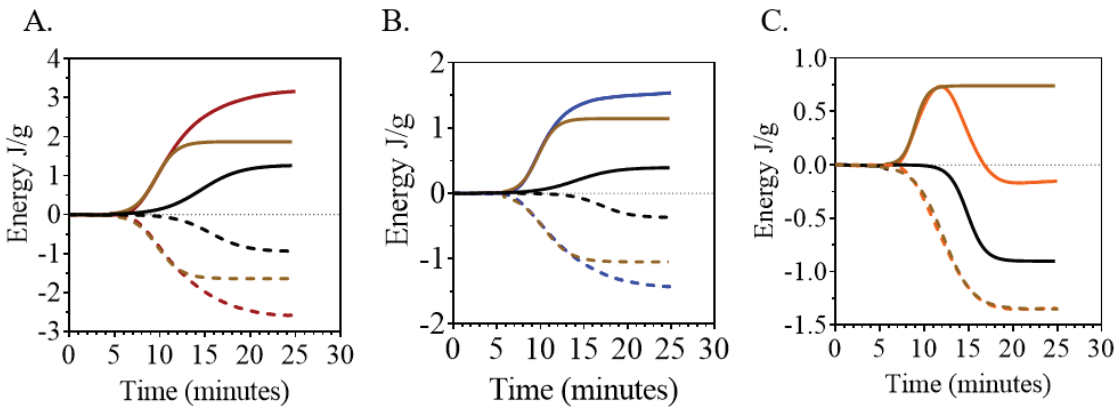

Figure 2-7: Deconvoluted s-shaped energy (J g-1) for (A-red) cumulative quantity for glycine, (B-blue) cumulative quantity for α-alanine, (C-orange) cumulative quantity for G3.5-COOH. Continuous line: probe/NO3- cycle, dashed-line: NO3-/ probe cycle, brown: reaction 1, black: reaction 2.

Table 2 - 2 Sorption/desorption total energy and kinetics of amino-bearing organic acids

	glycine		α-alanine		G3.5-COOH	
	Sorption	Desorption	Sorption	Desorption	Sorption	Desorption
Reaction-steps, *n*	2	2	2	2	2	1
Cumulative energy (J/g)	-3.14	2.59	-1.52	1.42	1.64	1.35
$E_{total\ 1}$	-1.87	1.65	-1.03	1.05	-0.74	1.35
$E_{total\ 2}$	-1.27	0.94	-0.49	0.37	0.90	-
Rate constants, k' (min^{-1})						
k'_1	0.38	0.33	0.42	0.28	0.63	0.27
k'_2	0.20	0.22	0.19	0.25	0.43	-
Half-life, $t_{1/2}$ (min)						
$t_{1/2,\ 1}$	9.92	10.14	9.70	10.54	9.20	11.99
$t_{1/2,\ 2}$	14.93	16.00	13.25	17.22	15.09	-

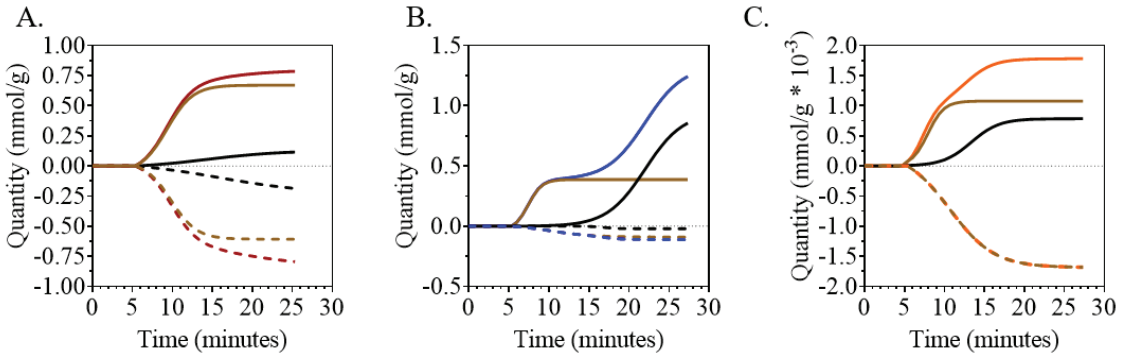

Figure 2-8: Deconvoluted s-shaped quantity (mmol g^{-1}) for (A-red) cumulative quantity for glycine, (B-blue) cumulative quantity for α-alanine, (C-orange) cumulative quantity for G3.5-COOH. Continuous line: probe/NO_3^- cycle, dashed-line: NO_3^-/ probe cycle, brown: reaction 1, black: reaction 2.

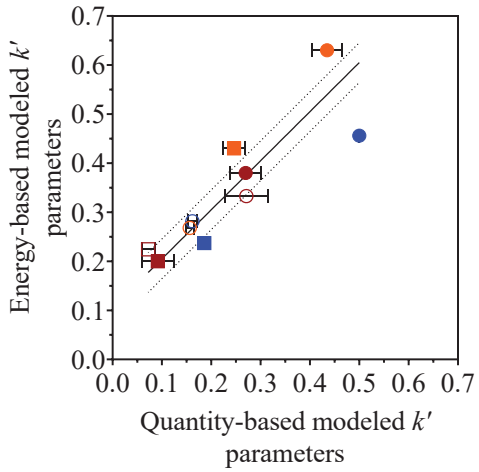

Figure 2-9: Comparison of reaction rate constants (k'rx) derived from energy data and quantity data. Filled symbols: sorption; unfilled symbols: desorption; circle: reaction 1; (square) reaction 2; red: glycine; blue: α-alanine; orange: G3.5-COOH.

Energetics of sorption/desorption

Table 2-3 shows the overall and step specific E_t, Q_{sorp}, and Q_{desorp} of glycine, α-alanine, and G3.5-COOH at the ferrihydrite-water interface. Using deprotonation information from Table 2-1, absolute molar heats of sorption (ΔH_{sorp}) and desorption (ΔH_{des}) were shown to be on the order of 0.61-22.4 kJ/mol of COO^- (Table 2-3). These values reflected a range of bonding mechanisms from a combination of van der Waals with ion exchange (< 2 kJ/mol), ion exchange (<10 kJ/mol), and ligand exchange (20-30 kJ/mol). An absolute ΔH_{sorp} value of 3.6 kJ/mol pointed to the reaction between glycine and NO_3^--saturated ferrihydrite occurring predominantly by ion exchange while absolute ΔH_{sorp} values of 1.24 kJ/mol and 1.69 kJ/mol for α-alanine and G3.5-COOH respectively were more in line with weak mixed van der Waals (induced dipole) and ion exchange (permanent dipole) bonding mechanism (Table 2-3). The exothermic nature of the glycine and α-alanine reactions pointed to their sorption being enthalpy-driven. On the other hand, the endothermic nature of the G3.5-COOH reaction pointed to its sorption being entropy-driven. This was well supported by calculated entropy at equilibrium ($\Delta G = 0$) and the experimental temperature of 22ºC. Here the entropy associated with the overall sorption (ΔS_{sorp}) of glycine, α-alanine, and G3.5-COOH was -12.4, - 4.21, and + 5.7 J/mol K respectively, pointing to increasing disorder at the ferrihydrite-water interface for glycine < α-alanine < G3.5-COOH (Table 2-3).

Molar heat of sorption (ΔH_{sorp}) and associated ΔS_{sorp} point to the first molecules of glycine, α-alanine, and G3.5-COOH going onto a well-ordered NO_3^--saturated ferrihydrite surface (reaction step 1), with glycine (ΔH_{sorp} = 2.58 kJ/mol) and α-alanine (ΔH_{sorp} = 2.43 kJ/mol) in the first step undergoing an ion exchange type process and G3.5-COOH (ΔH_{sorp} = 13.1 kJ/mol) undergoing a stronger, possibly mixed ion-ligand exchange (Table 2-3). Interestingly,

the calculated ΔS_{sorp} for the equilibrium case suggested that the ordering at the NO_3^-saturated ferrihydrite surface was significantly greater for G3.5-COOH sorption than glycine and α-alanine sorption. This comparatively more ordered interface could plausibly enable shorter-range, more inner sphere association between G3.5-COOH compared to weaker outer sphere associations of glycine and α-alanine in the first reaction step.

Disorder at the ferrihydrite-water interface increased during the second sorption/reaction step for α-alanine and G3.5-COOH, but decreased (increasing order) for glycine (Table 2-3). Despite disorder increasing for both α-alanine and G3.5-COOH in this second sorption step, an absolute ΔH_{sorp} value of 0.61 kJ/mol suggested that α-alanine formed more long-range, outer sphere mixed van der Waals and ion exchange type interaction compared to G3.5-COOH's absolute ΔH_{sorp} value of 22 kJ/mol that showed formation of shorter-range, inner sphere ligand exchange type interactions. Increasing order for glycine in this second sorption step favored a shorter range (stronger) more inner sphere exchange mechanism than that apparent from the first sorption step. It is also worth noting that the very different energy dynamics in step 2 points to the generally slower diffusion kinetics in this step being a result of steric effects arising from molecular size and entropic shifts plus shifts in chemodynamics from alteration in bonding mechanisms. Glycine also reportedly aligns its backbone perpendicular to sorbates' framework within the pores resulting in stabilized bonds and clogging and hindered diffusion of more molecules in the pores [57].

All endothermic ΔH_{desorp} obtained across reactions pointed to the desorption of glycine, α-alanine and G3.5-COOH from ferrihydrite by NO_3^- being an energy consuming, entropy-driven process. Glycine desorption from ferrihydrite by NO_3^- consumed 0.5-1 times the energy released during the sorption step (Table 2-3). Desorption for α-alanine consumed 4-28 times the energy

released in its sorption while that for G3.5-COOH desorption consumed 1-8 times the energy released in sorption. This desorption occurred spontaneously in an environment that involves an entropic shift/increased disorder of 1.5-30 times that of the interface during the sorption steps. It appears that energy shifts associated with reaction step 1 of the sorption and desorption dictate reversibility of sorption of the amino-bearing acids to ferrihydrite. For instance, despite their significant magnitudinal differences in ΔH_{sorp} and ΔH_{desorp} , all the sorbed glycine and G3.5-COOH were desorbed in the desorption phase. In both instances, the $\Delta H_{desorp}/\Delta H_{sorp}$ and associated entropic shift were 1 and 2 respectively; indicating that 1) the unit energy involved in the bond forming was equal to that consumed in bond breaking with the ferrihydrite surface; and 2) this was facilitated in an environment where disorder increased by a factor of 2 compared to the sorption state. Contrastingly, for α-alanine where only about 10% reversibility was observed, $\Delta H_{desorp}/\Delta H_{sorp}$ and entropic shift between sorption-desorption was 4 and 5 respectively, pointing to significantly higher energy demand and reorganization of the ferrihydrite-water interface to facilitate its complete desorption. That the energy dynamics and specifically of reaction step 1 would control the outcome is completely plausible given that this step would represent interactions in closest proximity to the ferrihydrite surface.

Table 2 - 3 Measured and calculated total energy, quantity, molar heat of reaction, and entropy for sorption and desorption reactions of amino-bearing organic acids onto/from ferrihydrite

	Total Energy, E_{total} (J/g)			Quantity (μmol/g)			Molar heat of reaction, ΔH (kJ/mol COO^-)			Entropy, ΔS (J/mol/K)		
	Overall	Reaction 1	Reaction 2	Overall	Reaction 1	Reaction 2	Overall	Reaction 1	Reaction 2	Overall	Reaction 1	Reaction 2
Sorption												
glycine	-3.13	-1.87	-1.26	856	727	135	-3.66	-2.58	-9.34	-12.4	-8.73	-31.6
α-alanine	-1.52	-1.02	-0.49	1221	421	800	-1.24	-2.43	-0.61	-4.21	-8.25	-2.08
G3.5-COOH	0.16	-0.74	0.90	1.86	1.08	0.785	1.69	-13.4	22.4	5.74	-45.4	76.0
Desorption												
glycine	2.59	1.64	0.94	852	645	208	3.03	2.55	4.53	10.3	8.6	15.3
α-alanine	1.42	1.05	0.37	127	106	21.0	11.2	9.92	17.4	37.8	33.6	59.0
G3.5-COOH	1.35	1.34		1.87	1.87		14.1	14.1		47.8	47.7	

Effect on ferrihydrite surface charge

Fig. 2-10 shows thermograms for the pre- and post-amino-bearing probe NO_3^-/Cl^- and Cl^-/NO_3^- exchange on ferrihydrite. Consistent with previous studies, NO_3^- replacing Cl^- (NO_3^-/Cl^-) on ferrihydrite was exothermic while Cl^- replacing NO_3^- (Cl^-/NO_3^-) was always endothermic with reactions lasting 10-15 minutes. Also consistent with a simple ion exchange, fully reversible process, the energy involved was equal for the forward and reverse reaction, i.e. E_{total} for NO_3^-/Cl^- exchange is equal to E_{total} for Cl^-/NO_3^-. This held true within each experiment. Comparison between anion exchange thermograms across amino-bearing organic acids indicated that sorption then desorption of glycine and G3.5-COOH resulted in increased E_{total} for post NO_3^-/Cl^- and Cl^-/NO_3^- on ferrihydrite. On the other hand, sorption then desorption of α-alanine had no effect (or only slightly decreased) E_{total} for NO_3^-/Cl^- and Cl^-/NO_3^- exchange on ferrihydrite. The increase in E_{total} for anion exchange post-glycine and G3.5-COOH was consistent with a 2-3 times increase in anion exchange while the absence of an effect on anion exchange post α-alanine was consistent with no change (or a slight decrease) in anion exchange sites. Irreversibly sorbed amino-bearing organic acid zwitterions (with the COO^- to the ferrihydrite surface and the NH_3^+ pointing away) in a 1:1 amino acid: charge ratio would be a plausible explanation for lack of effect on charge in α-alanine, but would not explain the apparent increase in anion exchange sites after the sorption then desorption of Glycine and G3.5-COOH from ferrihydrite. This could be for two reasons; Firstly, that glycine and G3.5-COOH were completely reversible ($Q_{sorp} = Q_{desorp}$); or secondly, that even with irreversibility an amino-acid: charge sorption ratio of 2 to 3 would be needed to account for observed differences between pre- and post-glycine and -G3.5-COOH, NO_3^-/Cl^- or Cl^-/NO_3^- E_{total}. Instead the most plausible explanation for glycine and G3.5-COOH-induced increase in anion exchange site on

ferrihydrite was pitting and crevice corrosion resulting in increased Fe edge sites with oxygen-deficiency and hence net positive charge.[58, 59] Given the observed changes in E_{total} between pre- and post-probe anion exchange, 2 or 3 additional oxygen-deficient, positively-charged Fe edge sites are produced per mole of desorbed glycine- or G3.5-derived carboxyl, respectively.

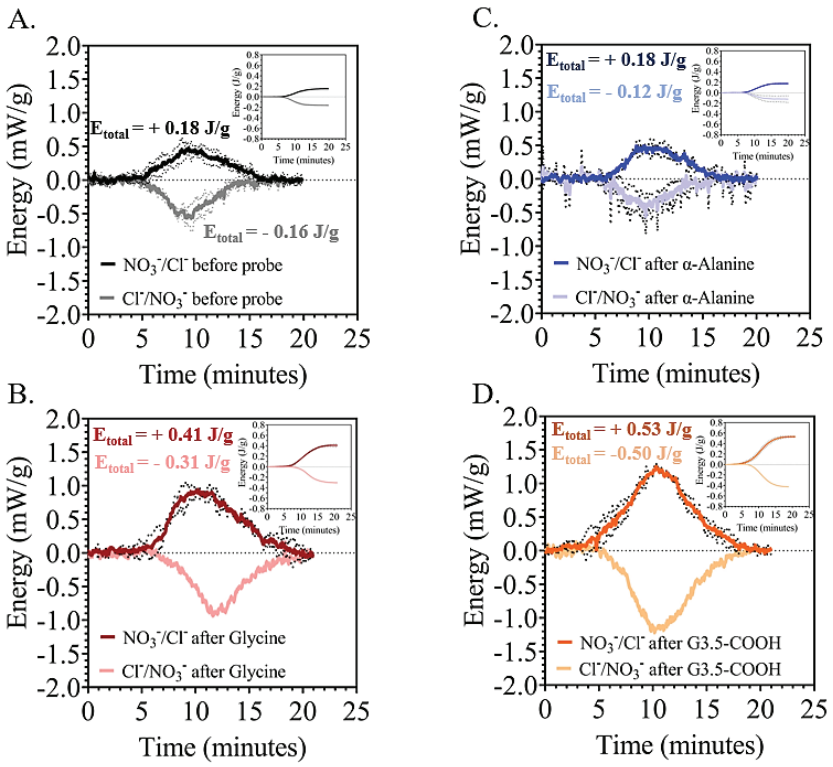

Figure 2-10: Anion exchange on ferrihydrite A: before amino-bearing organic acids treatment of ferrihydrite, B: after glycine treatment of ferrihydrite, C: after α-alanine treatment of ferrihydrite, D: after G3.5-COOH treatment of ferrihydrite.

CHAPTER 3: EFFECTS OF MOLECULAR CONFORMATION OF ALANINE ON SORPTION DYNAMICS, KINETICS, HEAT OF REACTION, AND SURFACE CHARGE OF FERRIHYDRITE

Introduction

Interactions between amino acids and inorganic compounds, such as metal oxides, are believed to have formed the first peptides [60]. A peptide bond/amide bond is formed between the α-nitrogen atom of one amino acid and the carbonyl carbon of a second. α-alanine is the simplest chiral amino acid present in nature and is typically chosen as a good model for studying biological systems that exhibit peptide bonding [56]. Like their predecessors, proteins can aggregate into insoluble abnormally larger structures during normal physiological conditions and in response to age or stress-induced protein misfolding and denaturation [61]. This aggregation is a recognized histopathological trait of Alzheimer's and Parkinson's disease and is also associated with several localized and systemic types of amyloidosis [62]. One approach to inhibit this is to synthesize short peptides that correspond to a self-recognition element (SRE) within the target sequence that drives fibril growth with subtle modifications so that the peptides can hydrogen-bond to the self-recognition site of the parent protein and block aggregation[63, 64]. Madine et. al[62] found that extending the backbone of a native SRE by replacing α-alanine with β-alanine decreased aggregation of α-synuclein in the hydrogen-bonding direction by 50% after a monitoring period of 7 days.

α-alanine is the simplest chiral proteinogenic amino acid used as a food additive and precursor for chemical and pharmaceutical products[35]. β-alanine is a non-proteinogenic amino acid incorporated in Vitamin B5 and employed in secondary metabolism in plants (lignin biosynthesis) [36]. The adsorption of α-alanine onto ferrihydrite at pH 5 was determined in Chapter 2 and found to be a two-step and enthalpy-driven process that occurred via a mixture of van der

Waals bonding and ion exchange reactions with a ΔH_{sorp} of -1.24 kJ mol^{-1}, and 10% reversibility by NO_3^- with no impact on ferrihydrite charge. The goal of this study was to investigate the shift in energetics and energy dynamics at the ferrihydrite—water interface induced by changing the position of the amine group in α-alanine from out-of-plane to in-plane with the carboxylic group, as observed in β-alanine.

Non-equilibrium transfer of α-alanine to ferrihydrite was observed in Chapter 2 and was attributed to α-alanine's ability to intra-aggregate [55] [56]. The difference in molecular conformation between α-alanine and β-alanine, namely the longer backbone of β-alanine, can be expected to alter the potential for intra-aggregation and hence interactions at the ferrihydrite-water interface. This would be reflected in its kinetics, with interactions anticipated to occur faster than in α-alanine. The location of the NH_2^+ group in β-alanine is also further away from its COO^- group; this would reduce repulsive forces between the amine group and the surface (NH_2^+ ····· M-OH^+) and facilitate stronger bonding in the β-alanine-ferrihydrite compared to its α-alanine-ferrihydrite counterpart. To test these hypotheses, a combined Flow adsorption microcalorimetry (FAMC)-Ultraviolet-visible spectroscopy (UV/vis) method was used to investigate and compare sorption/desorption dynamics of α-alanine versus β-alanine at the ferrihydrite-water interface. Specific focus was placed on their sorption/desorption dynamics, kinetics and energetics, as well as their post-sorption/desorption effects on ferrihydrite surface charge. All experiments were conducted at a solution pH of 5.

Materials and Methods

Ferrihydrite and Amino-acid solutions

Synthesis and characterization of the ferrihydrite used is covered in Chapter 2 and the Appendix. Selected physicochemical properties for α-alanine and β-alanine that would influence their sorption/desorption behavior are summarized in Table 3-1. At the experimental pH of 5, the surface of ferrihydrite would be predominantly (~99%) positively charged and would be expected to be involved in some electrostatic bonding with both amino acids which would be in their zwitterionic forms (Fig. 3-1). Molecular electrostatic potential (MEP) around the molecules was -0.89 at their deprotonated carboxylic group (i.e. $MEP_{COO^-} = -0.89$) and +0.90 at their protonated amine group ($MEP_{NH_3^+} = +0.90$). Concentrations of α-alanine and β-alanine were such that $[COOH]_{total} = 18.1mM$. That is, [α-alanine] = 18.1mM and [α-alanine] = 18.1mM.

Table 3 - 1 : Physicochemical properties of α-alanine and β-alanine interacting with ferrihydrite at pH 5

Amino acid	Molecular weight (g/mol)	pK_{a1}	pK_{a2}	Speciation at pH 5 (%)			Length (nm)	Width (nm)
				Cationic	Zwitterionic	Anionic		
α-alanine	89.1	2.34	9.69	0	100	0	0.50	0.35
β-alanine	89.1	2.34	9.69	0	100	0	0.60	0.35

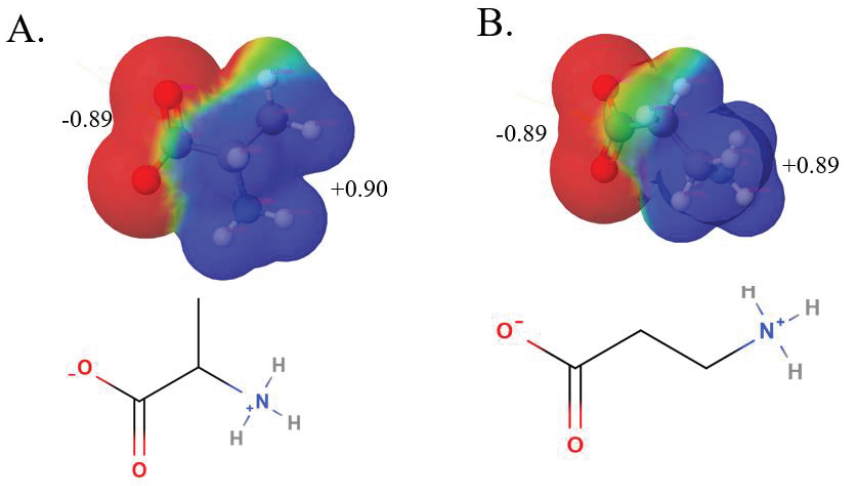

Figure 3-1: Distribution of molecular electrostatic potential (MEP) at pH 5 around (A) α-alanine and (B) β-alanine. At pH 5, the two molecules were in their zwitterionic form indicated by equal average positive charge and negative charge on the molecular simulations generated in MolView.

Experimental protocol and data handling

The same experimental and data handling protocols described in Chapter 2 and the appendix were used. Details are presented in these sections of the thesis. In brief, once initial thermal equilibrium and a NO_3^--saturated ferrihydrite surface was achieved, pre-probe anion exchange characteristics were assessed using two Cl^-/NO_3^- and two NO_3^-/Cl^- ion exchange cycles. After the second NO_3^-/Cl^- cycle and a return of the surface to NO_3^-- saturated ferrihydrite status, a single sorption cycle of the organic probe (α-alanine or β-alanine) was carried out until a return to thermal equilibrium, indicating full surface coverage of the ferrihydrite by α-alanine or β-alanine. This was then followed by a single "desorption" cycle and two cycles of post-probe Cl^-/NO_3^- and NO_3^-/Cl^- exchange. Effluent absorbance was continuously monitored in-tandem with FAMC measurements on both the sorption and desorption cycle.

Voltage versus time thermograms were used to assess reaction time, comparative magnitudes of energy change and whether the reactions were exothermic, endothermic, or mixed. Weight-adjusted energy (E_i; J/g), Q_{sorp}, and Q_{desorp} were used to assess the overall reaction (energy, sorption, desorption) dynamics, total reaction energy (E_{total}), total quantity sorbed (Q_{sorp}) and total quantity desorbed (Q_{desorp}). Deconvolution of E_i, Q_{sorp}, and Q_{desorp} was used to assess the number of reaction steps, their respective contribution to the total reaction, and respective rate constants.

In assessing the effects of α-alanine versus β-alanine on ferrihydrite surface charge, E_{total} (J/g) for pre-probe NO_3^-/Cl^- and Cl^-/NO_3^- behavior was quantitatively compared to that for post-probe NO_3^-/Cl^- and Cl^-/NO_3^-. This allowed for the assessment of whether sorption then desorption of α-alanine versus β-alanine at the ferrihydrite-water interface increased, decreased or had no effect on the quantity of anion exchange sites.

Results and Discussion

Sorption and desorption dynamics and kinetics:

Raw calorimetric response thermograms for α-alanine and β-alanine sorption onto NO_3^--saturated ferrihydrite are shown in Fig. 3-2 A. Thermograms for the desorption cycles (NO_3^- sorption to α-alanine and β-alanine-saturated ferrihydrite) are shown in Fig. 3-2 B. All thermograms were log-normal in shape with reaction times of 15-20 minutes. Thermograms indicated that α-alanine and β-alanine sorption onto NO_3^--saturated ferrihydrite occurred via an exothermic reaction while desorption was endothermic. The spontaneous occurrence of these reactions at the experimental temperature (22 ± 2.5ºC), with the requirement of a negative ΔG (where $\Delta G = \Delta H - T\Delta S$), suggested that the exothermic sorption reactions, which by convention carry a negative ΔH, required no increase in entropy/disorder (ΔS), while the endothermic desorption reactions, which carry a positive ΔH, required an increase in entropy of the system to facilitate spontaneous desorption.

Cumulative energy curves (Fig. 3-3 A) were consistent with enthalpy-driven sorption reactions and indicated that with E_{total} values of -1.52 J/g and -2.78 J/g for α-alanine and β-alanine respectively, the sorption of β-alanine onto a NO_3^--saturated ferrihydrite was a more spontaneous reaction compared to α-alanine's sorption by a factor of 1.8. On the other hand, entropy-driven desorption reactions (Fig. 3-3 B) were comparable for α-alanine (+ 1.42 J/g) and β-alanine (+ 1.75 J/g). Deconvolution of energy curves (Fig. 3-4) and quantity curves (Fig. 3-5) pointed to sorption and desorption reactions of both amino acids onto and from ferrihydrite occurring in two steps. Energy curves fitted with rate constants, *k'*, pointed to α-alanine and β-alanine being sorbed at similar rates with the first sorption step occurring faster than the second sorption step by a factor of 1.5-2.2 (Table 3-2). The desorption of β-alanine occurred at rates

similar to its sorption reaction steps, whereas the desorption of α-alanine was slower in the first desorption step compared to the first sorption steps of both amino acids and the first desorption step of β-alanine by a factor of 1.3-1.5. However, the reaction rates for two desorption steps of α-alanine were comparable (Table 3-2). This points to α-alanine's desorption occurring by a two-step desorption reaction with similar rates and mechanisms (k'_{sorp1} = 0.28 and $k'_{desorp2}$ = 0.25) as opposed to β-alanine's desorption occurring in fast and then slow-diffusion type desorption steps ($k'_{desorp1}$ = 0.40 and $k'_{desorp2}$ = 0.21).

Further, comparison of deconvoluted E_{total}, Q_{sorp}, and Q_{desorp} indicated that while α-alanine's sorption to NO_3^--saturated ferrihydrite was only partially reversible (10%) by NO_3^-, β-alanine's sorption was completely reversible by NO_3^-. Intra-aggregation of α-alanine with the surface is a plausible explanation for its significantly lower degree of reversibility (10%) compared to β-alanine (90%)[56, 62]. As observed in proteins [62], it is plausible that α-alanine's intra-aggregation with the surface is mediated by its constricted backbone while β-alanine's elongated backbone inhibits a similar mechanism.

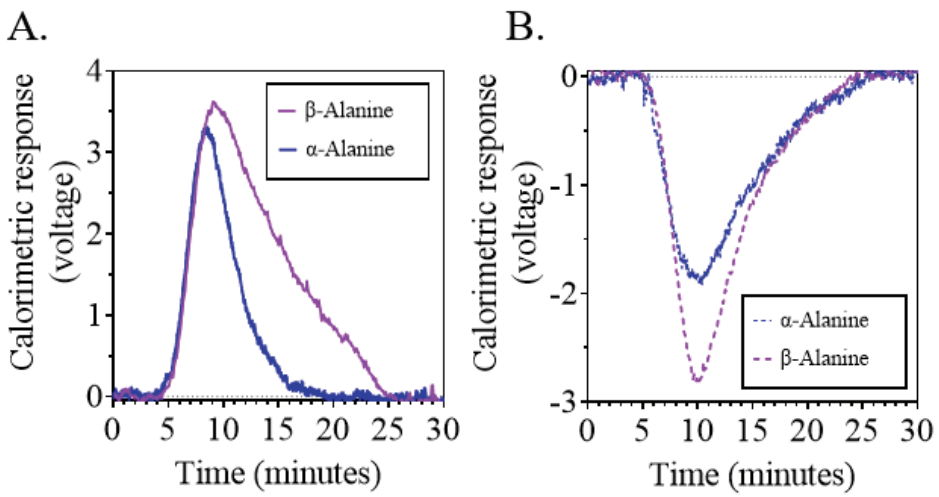

Figure 3-2: Calorimetric signals in voltage for (A) amino-acids/probe interacting with a nitrate (NO_3^-) saturated ferrihydrite and (B) NO_3^- interacting with a probe saturated ferrihydrite.

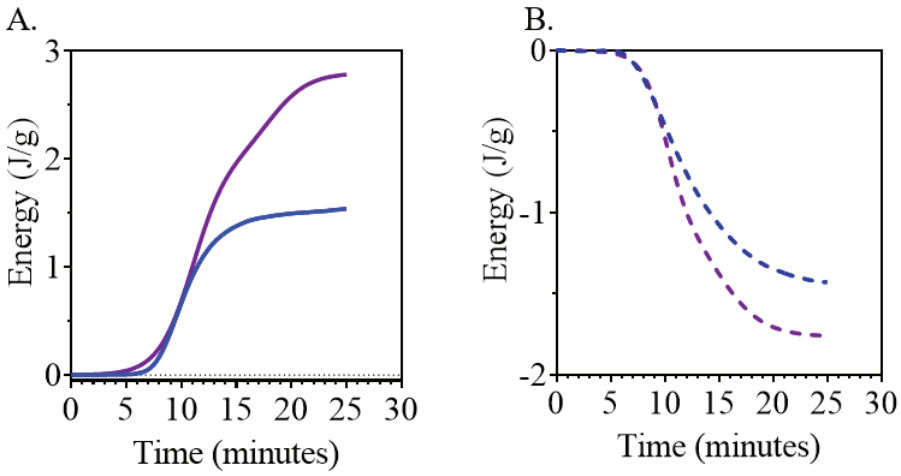

Figure 3-3: S-shaped energy peaks (J g^{-1}) for sorption (probe/NO_3^-) and desorption (NO_3^-/probe); blue: α-alanine, purple: β-alanine.

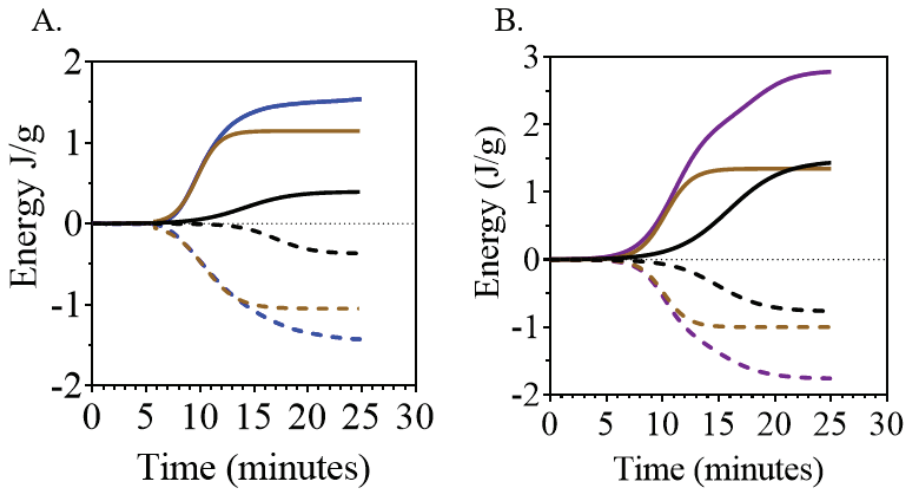

Figure 3-4: Deconvoluted s-shaped energy peaks (J g^{-1}) for (A-blue) cumulative energy for α-alanine, (B-purple) cumulative energy for β-alanine. Continuous line: probe/NO_3^- cycle, dashed-line: NO_3^-/ probe cycle, brown: reaction 1, black: reaction 2.

Table 3 - 2 Sorption/desorption total energy and kinetics of amino acids

	α-alanine		β-alanine	
	Sorption	Desorption	Sorption	Desorption
Reaction-steps, *n*	2	2	2	2
Cumulative energy (J/g)	-1.52	1.42	-2.44	1.75
$E_{total\ 1}$	-1.03	1.05	-1.34	0.99
$E_{total\ 2}$	-0.49	0.37	-1.43	0.76
Rate constants, k' (min^{-1})				
k'_1	0.42	0.28	0.37	0.40
k'_2	0.19	0.25	0.18	0.21
Half-life, $t_{1/2}$ (min)				
$t_{1/2,\ 1}$	9.70	10.54	10.24	10.11
$t_{1/2,\ 2}$	13.25	17.22	15.89	14.92

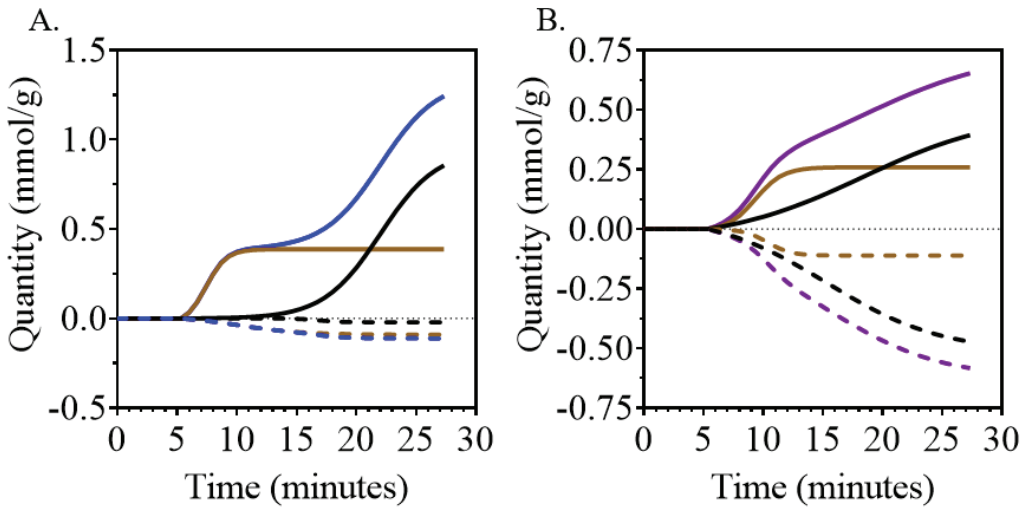

Figure 3-5: Deconvoluted s-shaped quantity (mmol g^{-1}) for (A-blue) cumulative energy for α-alanine, (B-purple) cumulative energy for β-alanine. Continuous line: probe/NO_3^- cycle, dashed-line: NO_3^-/ probe cycle, brown: reaction 1, black: reaction 2.

Energetics of sorption/desorption:

Table 3-3 shows the overall and step specific E_t, Q_{sorp}, Q_{desorp} of α-alanine and β-alanine at the ferrihydrite-water interface. Using deprotonation information from Table 3-1, absolute molar heats of sorption (ΔH_{sorp}) and desorption (ΔH_{desorp}) were shown to be on the order of 0.61-17.4 kJ/mol COO^-, reflecting a range of bonding mechanisms from a combination of van der Waals with ion exchange (< 2 kJ/mol), ion exchange (<10 kJ/mol), and long-range type ligand exchange (20-30 kJ/mol). Absolute ΔH_{sorp} values pointed to the sorption reaction of α-alanine (ΔH_{sorp} = 1.24 kJ/mol) occurring by a weak mixed van der Waals (induced dipole)-ion exchange (permanent dipole) bonding mechanism while that for β-alanine (ΔH_{sorp} = 3.7 kJ/mol) occurred predominantly by ion exchange. The exothermic nature of the glycine and α-alanine reactions pointed to their sorption being enthalpy-driven. The calculated entropy values at equilibrium (ΔG = 0) and at the experimental temperature of 22 ºC associated with the overall sorption (ΔS_{sorp}) for α-alanine and β-alanine were - 4.21 and - 12.51 J/mol/K respectively pointing to far less disorder at the ferrihydrite-water interface in β-alanine compared to α-alanine.

Molar heat of sorption (ΔH_{sorp}) and associated ΔS_{sorp} pointed to the first molecules of α-alanine and β-alanine going onto a well-ordered NO_3^--saturated ferrihydrite surface (reaction step 1). ΔH_{sorp} values for α-alanine (- 2.43 kJ/mol) and β-alanine (- 5.0 kJ/mol) in this first sorption step pointed to an ion exchange type process appearing to be much stronger process in β-alanine. The calculated ΔS_{sorp} for the equilibrium case suggested that the ordering at the NO_3^--saturated ferrihydrite surface was comparatively greater for β-alanine sorption than α-alanine sorption (Table 3-3), which most likely allowed β-alanine to form stronger bonds with the surface as opposed to α-alanine's weaker associations.

Disorder at the ferrihydrite-water interface increased during the second sorption/reaction step for both amino acids (Table 3-3). This resulted in a change from a shorter-range to longer-range ion exchange bonds for β-alanine with absolute ΔH_{sorp} values of 5 kJ/mol and 3 kJ/mol for reaction 1 and reaction 2 respectively while, α-alanine exhibited a change from ion exchange to outer sphere mixed mixed van der Waals and ion exchange type interaction with absolute ΔH_{sorp} values of 2.43 kJ/mol and 0.61 kJ/mol for reaction 1 and reaction 2 respectively. It is worth noting that the maintained ion exchange-type mechanism for β-alanine in sorption reaction 1 and reaction 2 despite the latter being a diffusion-type mechanism (k'_{rx1} = 0.42 vs k'_{rx2} = 0.19, Table 3-2) points to the reported arrangement of β-alanine parallel to the adsorbent's wall in the pores reducing steric effects and facilitating more molecules to penetrate the pores in an ion exchange mechanism [57]. In contrast, α-alanine steric hindrances associated with its constricted and short backbone [57] are most likely responsible for weaker bonds formed in this sorption step 2, most likely in the hydrogen bond direction as previously discussed.

Endothermic ΔH_{desorp} values for both amino-acids reactions pointed to the desorption of α-alanine and β-alanine from ferrihydrite by NO_3^- being an energy consuming, entropy-driven process. Desorption of α-alanine from ferrihydrite consumed 4-28 times the energy released in its sorption (Table 3-3) while that for β-alanine consumed 0.5-1.8 times the energy released during sorption. It appeared that the energy shifts associated with reaction step 2 of the sorption and desorption reactions dictated the overall energetics of β-alanine sorption and desorption onto/from ferrihydrite. This is plausible because β-alanine underwent more adsorption into the pores in reaction step 2 (Q_{bind} = 483 μmol/g) compared to that on the surface in reaction step 1 (Q_{bind} = 268 μmol/g). The $\Delta H_{desorp}/\Delta H_{sorp}$ and associated entropic shift for this reaction step 2 of β-alanine was 0.5 and 1.5 respectively, indicating that 1) the unit energy involved in the bond forming was much less than that consumed in bond breaking with the ferrihydrite surface; and 2)

this was facilitated in an environment where disorder increased by a factor of 1.5 compared to the sorption state. Contrastingly, for α-alanine where only about 10% reversibility was observed, the energy associated with reaction step 1 appeared to dictate the overall energetics of α-alanine's interactions with ferrihydrite (Table 3-3). This reaction step 1 indicated that $\Delta H_{desorp}/\Delta H_{sorp}$ and entropic shift between sorption-desorption was 4 and 5 respectively, pointing to significantly higher energy demand and reorganization of the ferrihydrite-water interface to facilitate α-alanine's complete desorption.

Table 3 - 3 Measured and calculated total energy, quantity, molar heat of reaction, and entropy for sorption and desorption reactions of amino acids onto/from ferrihydrite

	Total Energy, E_{total} (J/g)			Quantity (μmol/g)			Molar heat of reaction, ΔH (kJ/mol COO^-)			Entropy, ΔS (J/mol/K)		
	Overall	Reaction 1	Reaction 2	Overall	Reaction 1	Reaction 2	Overall	Reaction 1	Reaction 2	Overall	Reaction 1	Reaction 2
Sorption												
α-alanine	-1.52	-1.02	-0.49	1221	421	800	-1.24	-2.43	-0.61	-4.21	-8.25	-2.08
β-alanine	-2.78	-1.35	-1.43	750	268	483	-3.71	-5.0	-3.0	-12.56	-17.1	-10.1
Desorption												
α-alanine	1.42	1.05	0.37	127	106	21.0	11.2	9.92	17.4	37.8	33.6	59.0
β-alanine	1.76	1.00	0.76	670	112	559	2.6	8.9	1.36	8.9	30.3	4.6

Effect on ferrihydrite surface charge

Thermograms for pre- and post-amino acids NO_3^-/Cl^- and Cl^-/NO_3^- anion exchanges on ferrihydrite are shown in Fig. 3-6. Comparison between anion exchange thermograms across amino acids indicated that sorption then desorption of β-alanine resulted in increased E_{total} by a factor of ≈ 2 for post NO_3^-/Cl^- and Cl^-/NO_3^- exchanges on ferrihydrite. On the other hand, sorption then desorption of α-alanine as previously discussed in Chapter 2 had no effect (or showed only slight decrease) on E_{total} for NO_3^-/Cl^- and Cl^-/NO_3^- exchange on ferrihydrite. β-alanine's high reversibility (90%) compared to α-Alanine's slight reversibility (10%) points back to previously observed mechanisms in Chapter 2 of irreversibly sorbed amino-bearing organic acids having no effect (or slight decrease) in E_{total} for NO_3^-/Cl^- and Cl^-/NO_3^- exchange on ferrihydrite while reversibly bound amino-bearing organic acids increase E_{total} for NO_3^-/Cl^- and Cl^-/NO_3^- exchange on ferrihydrite. β-alanine's increase in E_{total} by a factor of 2 falls in line with an increased E_{total} between pre- and post-probe anion exchange of 2 - 3 observed in Chapter 2 for the completely reversible glycine and G3.5-COOH. This then indicates that β-alanine was behaving more like glycine and G3.5-COOH and its desorption corroded the surface leaving behind more Fe edge sites that are oxygen deficient with net positive sites charges [58, 59] increasing post anion exchange E_{total} as a result.

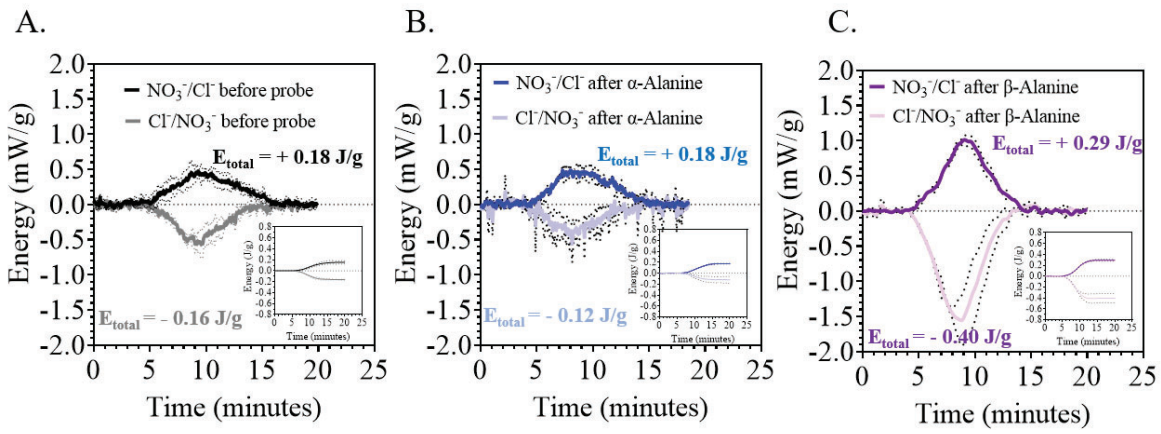

Figure 3-6: Anion exchange energy on ferrihydrite A: before amino-bearing organic acids treatment of ferrihydrite, B: after α-alanine treatment of ferrihydrite, (B) after β-alanine treatment of ferrihydrite.

CHAPTER 4: EFFECTS OF HYDROLIZABILITY ON SORPTION DYNAMICS, KINETICS, HEAT OF REACTION, AND SURFACE CHARGE OF FERRIHYDRITE

Introduction

Minerals play an important role in the bioavailability and cycling of nutrients in biogeochemical cycles. Adsorption of organic phosphorous-type molecules to environmental particles is assumed to limit enzymatic hydrolysis and phase transformation from organic phosphorous (Po) to inorganic phosphorous (Pi), a reaction preceding phosphorus uptake by plants and microorganisms [65]. Olsson et. al reported otherwise in their findings that the rate of enzymatic hydrolysis of glucose-1-phosphate (G1P) adsorbed on goethite by acid phosphatase (AcPase) was on the same order of magnitude as in aqueous solution [65]. Contrary to enzyme mediated-dephosphorylation found to occur on a time-scale of hours [66-68], Klein et. al observed that ferrihydrite-mediated dephosphorylation of a suite of ribonucleotides occurred on a time-scale of days [69].

Building on the findings of the aforementioned studies, the objective of the present study was to use a combined method of Flow adsorption microcalorimetry (FAMC)-Ultraviolet visible spectroscopy (UV/vis) to extract information regarding the effect of hydrolysis of organic molecules on sorption/desorption dynamics, kinetics, heat of reaction, and change in surface charge at the ferrihydrite-surface interface at pH 5. Adenosine triphosphate disodium (ATP) is a ubiquitous nucleotide that acts as a reservoir and energy conveyer in terrestrial and marine photosynthetic processes [37], and a source of Po in natural soils and sediments [70, 71]. ATP consists of an adenine base bound to a ribose molecule, which is bound to a triphosphate unit at the 5th position of the ribose (Fig. 4-1). Depending on the pH environment, the terminal phosphate and nitrogen of the base (N-7) dictate the dominant species and sorption behavior of ATP.

The adsorption of a sturdy/nonhydrolyzable-ATP analog, Poly amidoamine dendrimer G3.5-COOH onto ferrihydrite at pH 5 was determined in Chapter 2 and found to be an electrostatic reversible reaction that increases surface charge by pitting. FAMC-UV/vis adsorption data of G3.5-COOH onto ferrihydrite identified two stages; an initial enthalpy-driven sorption reaction, followed by a slower entropy-driven reaction with the surface. Unlike G3.5-COOH, adsorption of ATP is expected to be a driven by two compounds (Po and Pi) because the hydrolysis of ATP can sequentially generate Pi and ribonucleotides with different Po moieties as shown by the equation below:

$$ATP \rightarrow ADP + Pi \rightarrow AMP + Pi \rightarrow Adenosine + Pi \qquad [4\text{-}1]$$

where Pi is inorganic phosphorous and ATP, ADP, and AMP are adenosine monophosphate, diphosphate, and triphosphate respectively. Klein et. al reported that at pH 7, ferrihydrite mediated the dephosphorylation of ≈ 15% of the initial ATP within a 10-day reaction time (generating ADP and AMP), and attributed missing ATP to adsorption on the surface [69]. ATP-ferrihydrite interaction in this study is expected to occur through an adsorption reaction onto the surface, followed by a slower ferrihydrite-mediated Pi generation and adsorption. Using flow adsorption calorimetry like the technique used in this study, Harvey et. al noted that at pH 4.8 Pi sorption on Al(III) subsituted–Fe(III) hydr(oxide) occurred irreversibly on anion exchange sites with molar heats of reactions ten times that for anion exchange (−25 and −39 kJ/mol) [31]. In natural systems, this trapped Pi can become available upon mineral weathering, dissolution, or exchange reactions [72, 73]. In this study, recovering of this trapped Pi by an anion exchange reaction is expected to be a high energy and slow irreversible reaction that will decrease anion exchange sites on ferrihydrite.

Materials and Methods

Ferrihydrite and Organic acid solutions

Synthesis and characterization of the ferrihydrite used is covered in Chapter 2 and the appendix. Selected physicochemical properties of G3.5-COOH and ATP that would influence their sorption/desorption behavior are summarized in Table 4-1. Although the two molecules have comparable pK_{a1} and pK_{a2} (Table 4-1), ATP is a phosphate-type organic molecule that is 80% uncharged, 16% cationic, and 4% anionic at pH 5, while G3.5-COOH is a carboxylic-type organic molecule that is 76 % zwitterionic, 24 % cationic, and 4% anionic at pH 5 (see appendix). The molecular electrostatic potential (MEP) around the G3.5-COOH decreased from the deprotonated terminal carboxylic groups (COO^-) to the protonated tertiary amine groups (NH_2^+), while for ATP MEP decreased from the triphosphate unit to the adenine base (Fig. 4-1). Concentrations of molecules were such that $[COO^-/H_2PO_3^-]_{total}$ = 18.1mM i.e. [G3.5-COOH] = $2.8*10^{-2}$ mM and [ATP] = 18.1mM. At the experimental pH of 5, G3.5-COOH and ATP were interacting with a predominantly positively charged ferrihydrite (~99%).

Table 4 - 1 Physicochemical properties for G3.5-COOH and ATP interacting with ferrihydrite at pH5

Amino-based organic acid	Molecular weight (g/mol)	pK_{a1}	pK_{a2}	Speciation at pH 5 (%)			
				Cationic	Zwitterionic	Anionic	Uncharged
G3.5-COOH	12931	4.5	6.3	24	76	4	
ATP	551.14	4.3	6.5	16		4	80

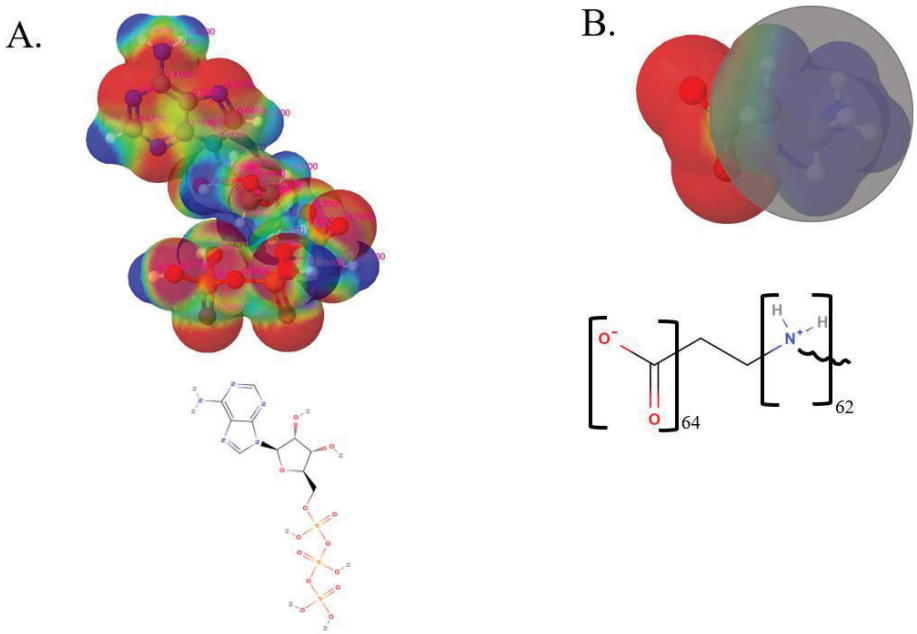

Figure 4-1: Distribution of molecular electrostatic potential (MEP) at pH 5 around (A) Adenosine triphosphate (ATP) and (B) poly amidoamine dendrimer G3.5-COOH. Molecular simulations were generated in MolView.

Experimental protocol and data handling

The same experimental and data handling protocols described in Chapter 2 and the appendix were used. Details are presented in these sections of the thesis. In brief, once initial thermal equilibrium and a NO_3^--saturated ferrihydrite surface was achieved, pre-probe anion exchange characteristics were assessed using two Cl^-/NO_3^- and two NO_3^-/Cl^- ion exchange cycles. After the second NO_3^-/Cl^- cycle and a return of the surface to NO_3^-- saturated ferrihydrite status, a single sorption cycle of the organic probe (G3.5-COOH or ATP) was performed until a return to thermal equilibrium was achieved, indicating full surface coverage of the ferrihydrite by G3.5-COOH or ATP. This was then followed by a single "desorption" cycle and two cycles of post-probe Cl^-/NO_3^- and NO_3^-/Cl^- exchange. Effluent absorbance was continuously monitored in-tandem with FAMC measurements on both the sorption and desorption cycle. For ATP, the ascorbic acid solution-based analysis [74] of the effluents was also conducted to monitor hydrolysis of ATP to P_i.

Voltage versus time thermograms were used to assess reaction time, comparative magnitudes of energy change and whether the reactions were exothermic, endothermic, or mixed. Weight-adjusted energy (E_i; J/g), Q_{sorp}, and Q_{desorp} were used to assess the overall reaction (energy, sorption, desorption) dynamics, total reaction energy (E_{total}), total quantity sorbed (Q_{sorp}) and total quantity desorbed (Q_{desorp}). Deconvolution of E_i, Q_{sorp}, and Q_{desorp} was used to assess the number of reaction steps, their respective contribution to total reaction, and respective rate constants.

In assessing the effects of G3.5-COOH versus ATP on ferrihydrite surface charge, E_{total} (J/g) for pre-probe NO_3^-/Cl^- and Cl^-/NO_3^- behavior was quantitatively compared to that for post-probe NO_3^-/Cl^- and Cl^-/NO_3^-. This allowed for the assessment of whether sorption then

desorption of G3.5-COOH and ATP at the ferrihydrite-water interface increased, decreased or had no effect on the quantity of anion exchange sites.

Results and Discussion

Sorption and desorption dynamics and kinetics:

Raw calorimetric response thermograms for ATP and G3.5-COOH onto NO_3^--saturated ferrihydrite at pH 5 are shown in Fig. 4-2 A. Thermograms for the reverse reaction (i.e. NO_3^- sorption to ATP and G3.5-COOH -saturated ferrihydrite) are shown in Fig. 4-2 B. Thermograms for sorption and desorption of G3.5-COOH were log-normal in shape with reactions lasting 15 minutes, consistent with simple ion exchange reactions on metal oxides [31, 46]. Similarly, ATP thermograms were log-normal shaped but extended in time with ATP sorption and desorption lasting 30 and 160 minutes respectively. These long reaction times are similar to those observed in phosphate sorption on Al-Fe co-precipitated hydr(oxides) [31] and arsenic sorption on amorphous aluminum hydroxide [46] via ligand exchange.

Differential voltage thermograms pointed to ATP sorption to NO_3^--saturated ferrihydrite occurring via purely exothermic reaction steps. In contrast, sorption of G3.5-COOH to NO_3^--saturated ferrihydrite was mixed with the first half being exothermic and the other half being endothermic. Given the spontaneous nature of the reactions at the experimental temperature (22 ± 2.5° C) and the requirement of spontaneous reactions having $-\Delta G$ (where $\Delta G = \Delta H - T\Delta S$) it is reasonable to postulate that for ATP its exothermic sorption, which by convention carries a $-\Delta H$ value, required no increase in entropy (ΔS) of the system to facilitate sorption. By contrast, the spontaneous sorption observed for G3.5-COOH with its endothermic sorption ($+\Delta H$) would require an increase in entropy of the system. The endothermic nature of NO_3^- interacting with

G3.5-COOH and ATP-saturated ferrihydrite, which carries a + ΔH, indicates that spontaneous desorption of these organic acids from ferrihydrite by NO_3^- at pH 5 required increased entropy. That is, while the sorption for ATP to NO_3^--saturated ferrihydrite is enthalpy-driven, that for G3.5-COOH and the desorption of both molecules from ferrihydrite by NO_3^- is entropy-driven at the experimental conditions (22 ± 2.5° C).

Cumulative energy curves (Fig. 4-3) were in agreement with enthalpy-driven ATP sorption (ΔH_{sorp} = - 8.5 J/g) as opposed to entropy-driven G3.5-COOH sorption (ΔH_{sorp} = + 0.16 J/g). By contrast, desorption of ATP (ΔH_{desorp} = + 11.6 J/g) was more entropy-driven than the desorption of G3.5-COOH (ΔH_{desorp} = + 1.35 J/g); i.e. more disorder was required for the desorption of ATP to occur spontaneously at the experimental temperature (22°C). This was very well in agreement with the formation of strong bonds via an inner sphere ligand exchange mechanism in the ATP sorption reaction, forming much harder bonds to break as opposed to G3.5-COOH's weaker ion exchange associations with the surface in the sorption step. In agreement with the log-normal shape of heat flow thermograms, fitted rate constants (k') pointed to ATP and G3.5-COOH sorption to NO_3^--saturated ferrihydrite in a first fast reaction step followed by a second slow reaction step (Table 4-2). During this sorption reaction some ATP notably hydrolyzed and produced inorganic phosphorous (Pi) as evidenced by Pi concentrations in effluents being higher than background concentrations measured in the starting solution (Fig. 4-6 A). At pH 4-5, Pi has been shown to form a bidentate complex with Fe-hydroxides [75]. Consequently, the sorption of ATP onto NO_3^--saturated ferrihydrite occurred via surface interactions with hydrolyzed and non-hydrolyzed ribonucleotides (termed AXP hereafter) and Pi (Fig. 4-5).

Fitted rate constants (*k'*) pointed to the non-hydrolysable G3.5-COOH sorbing onto ferrihydrite much faster (by an order of magnitude) compared to AXP and Pi sorption reactions (Table 4-2). AXP and Pi rate constants were more comparable to each other with AXP's rate of sorption only 1.5 times faster than Pi (Table 4-2). This was in agreement with a recent study suggesting sorption of ATP onto ferrihydrite preceding slow ferrihydrite-mediated hydrolysis [69]. While the desorption of G3.5-COOH from ferrihydrite occurred slower in a single reaction step (Table 4-2, Fig 4-4 B & D); desorption rates of AXP and Pi were comparable to their sorption rates (Table 4-2) with Pi desorbing in a three step reaction (Fig. 4-5 B & D) generating a near 7-fold greater amount of Pi compared to the sorption stage (Fig. 4-4 B).

Comparison of deconvoluted E_i, Q_{bind}, and Q_{debind} further pointed to G3.5-COOH sorption to NO_3^--saturated ferrihydrite being completely reversible by NO_3^-. AXP sorption on the other hand was only partially (≈ 84%) reversible by NO_3^-. The missing AXP was most likely involved in the generation of Pi in both the sorption and desorption phase. NO_3^- exchange for previously bound AXP (84%) in the desorption reaction could have also contributed in the generation of the surplus Pi during the desorption phase.

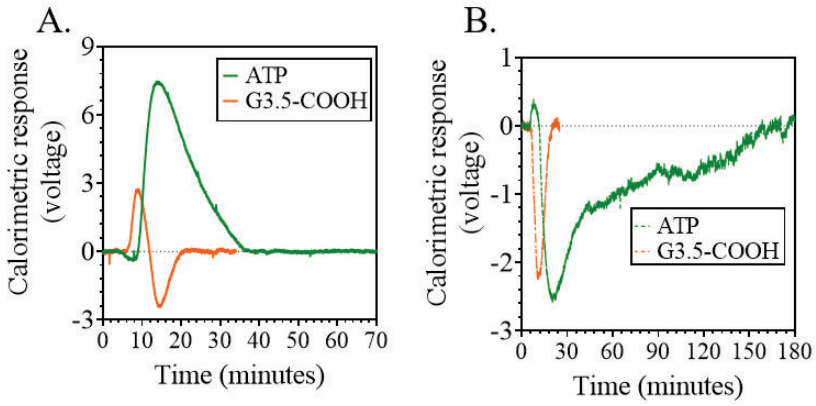

Figure 4-2: Calorimetric signals in voltage for (A) organic acids interacting with a nitrate (NO_3^-) saturated ferrihydrite (B) NO_3^- interacting with a probe-saturated ferrihydrite.

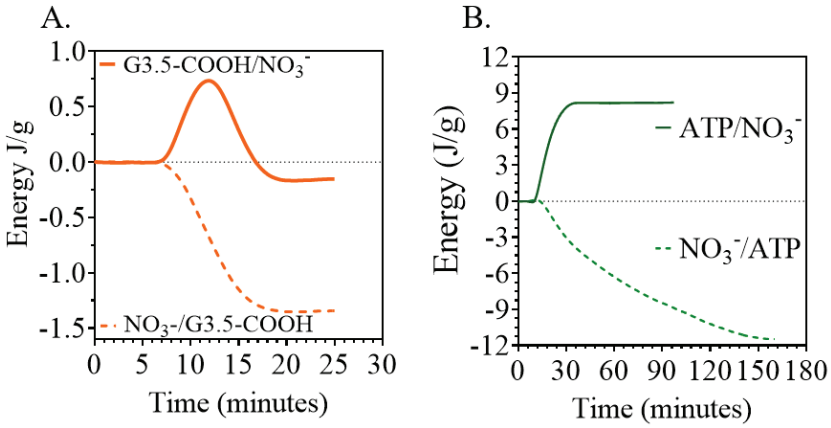

Figure 4-3: Cumulative energy peaks (J/g) for (A) G3.5-COOH sorption (continuous line) and desorption (dashed-line) onto/from ferrihydrite. (B) ATP sorption (continuous line) and desorption (dashed-line) onto/from ferrihydrite.

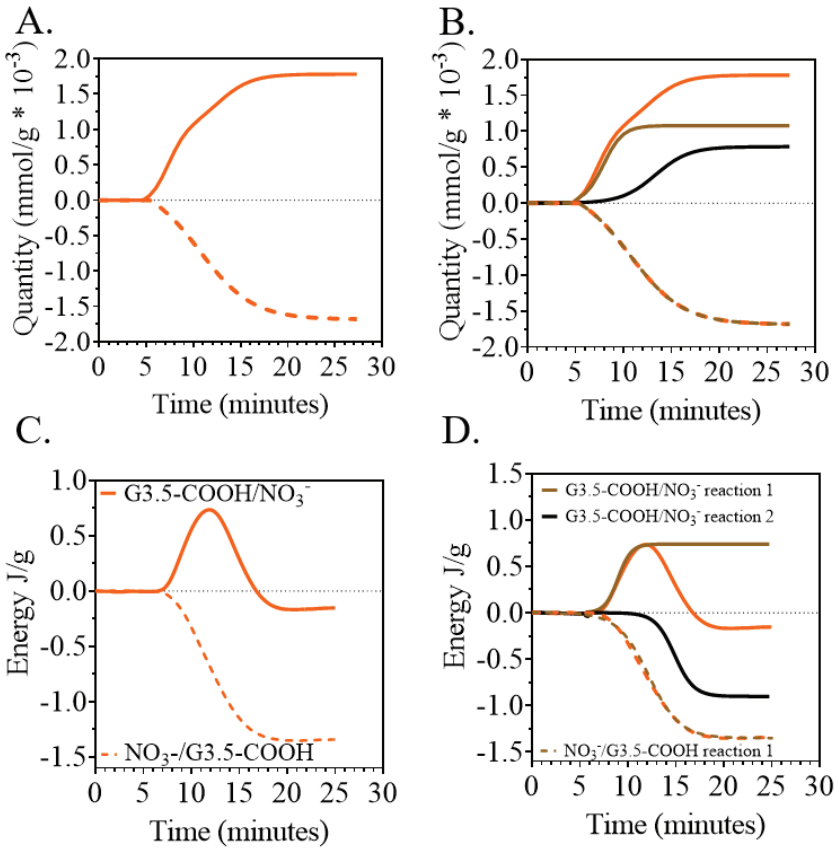

Figure 4-4: Quantity and energy for G3.5-COOH interaction with ferrihydrite. (A & B) quantity in mmol/g, (C & D) energy in J/g, (orange) cumulative, (brown) reaction 1, (black) reaction 2, (continuous line) sorption, (dashed-line) desorption.

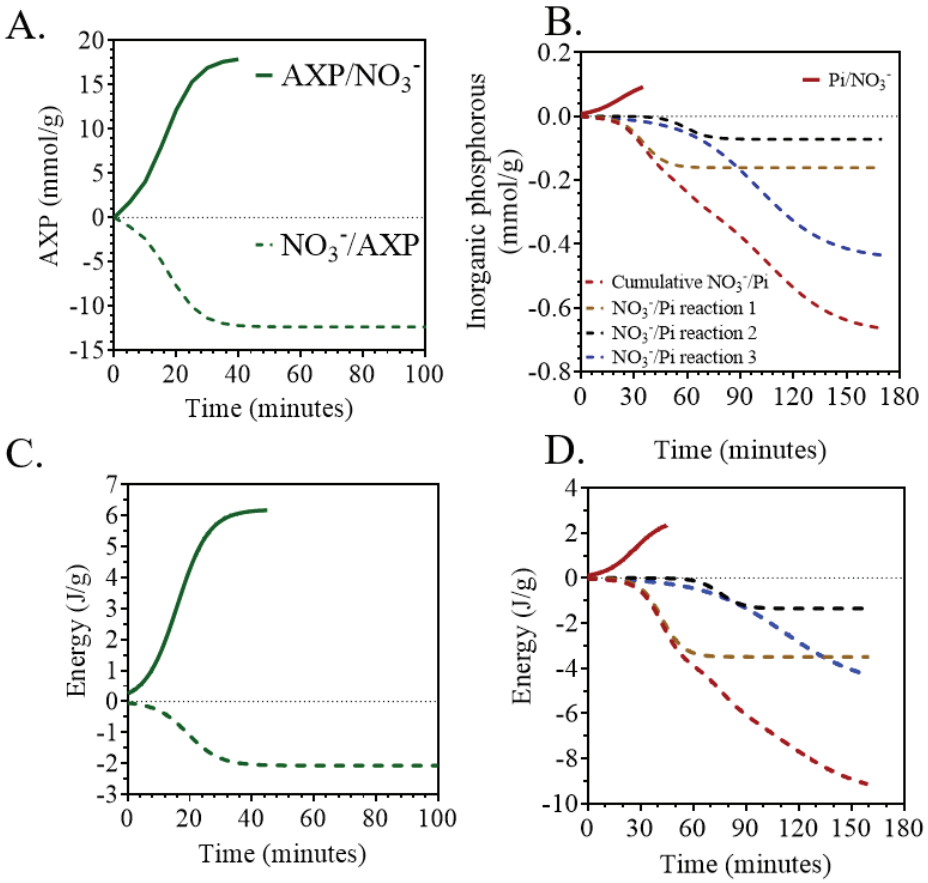

Figure 4-5: Quantity and energy for ATP interaction with ferrihydrite. (A) quantity of AXP in mmol/g, (B) quantity of inorganic phosphorous (Pi) in mmol/g, (C) energy for sorption and desorption of AXP, (D) energy for sorption and desorption of Pi, (continuous line) sorption, (dashed-line) desorption, (brown) reaction 1, (black) reaction 2, (blue) reaction 3.

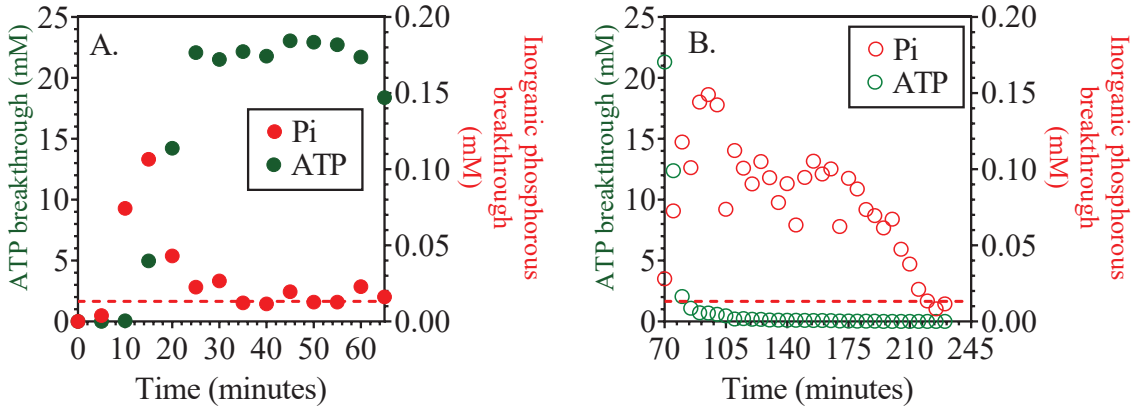

Figure 4-6: Concentrations of inorganic phosphorous and AXP in effluents during (A) the sorption phase and (B) the desorption phase. Red-dashed line shows background inorganic phosphate measured in solution.

Table 4 - 2 Sorption/desorption total energy and kinetics of organic acids onto/from ferrihydrite

	G3.5-COOH		ATP			
			AXP		Pi	
	Sorption	Desorption	Sorption	Desorption	Sorption	Desorption
Reaction-steps, n	2	1	1	1	1	3
Cumulative energy (J/g)	0.16	1.35	-6.2	2.47	-2.62	9.68
$E_{total\ 1}$	-0.74	1.35	-6.20	2.47	-2.62	3.50
$E_{total\ 2}$	0.90	-	-	-	-	1.35
$E_{total\ 3}$			-	-	-	4.83
Rate constants, k' (min^{-1})						
k'_1	0.63	0.27	0.09	0.08	0.05	0.07
k'_2	0.43	-	-	-	-	0.07
k'_3			-	-	-	0.02
Half-life, $t_{1/2}$ (min)						
$t_{1/2,\ 1}$	9.20	11.99	16.00	19.36	27.00	42.0
$t_{1/2,\ 2}$	15.09		-	-	-	75.5
$t_{1/2,\ 3}$	-	-	-	-	-	112.0

Energetics of sorption/desorption

Table 4-3 and Table 4-4 show the overall and step specific E_t, Q_{bind} and Q_{debind} respectively of G3.5-COOH and ATP (AXP and Pi) at the ferrihydrite-water interface. Using deprotonation information from Table 4-1, absolute molar heats of sorption (ΔH_{sorp}) and desorption (ΔH_{desorp}) were shown to be on the order of 1.7-22.4 kJ/mol COO^- for the G3.5-COOH, 0.2-0.4 kJ/mol for AXP, and 9.9-25.3 kJ/mol for Pi. These values reflected a range of bonding mechanisms from a combination of van der Waals with ion exchange (< 2 kJ/mol), ion exchange (<10 kJ/mol), and ligand exchange (20-30 kJ/mol). Absolute ΔH_{sorp} values pointed to the reaction G3.5-COOH (ΔH_{sorp} = 1.69 kJ/mol) and AXP (ΔH_{sorp} = 0.4 kJ/mol) at NO_3^--saturated ferrihydrite occurring predominantly by weaker mixed van der Waals (induced dipole)-ion exchange (permanent dipole) bonding mechanisms, while that of Pi (ΔH_{sorp} = 25.3 kJ/mol) was more in line with inner sphere ligand exchange bond formation with the surface. The one step exothermic nature of the AXP and Pi sorption reactions onto ferrihydrite pointed to their sorption being enthalpy-driven. On the other hand, the mixed exothermic and endothermic nature of the G3.5-COOH reaction pointed to its sorption being enthalpy driven first and then shifting to an entropy-driven sorption reaction. This was well supported by calculated entropy at equilibrium (ΔG = 0) and the experimental temperature of 22ºC. Here the entropy associated with the overall sorption (ΔS_{sorp}) of AXP, Pi, and G3.5-COOH was -1.2, - 85.9, and + 5.7 J/mol K respectively, pointing to increasing disorder at the ferrihydrite-water interface for Pi < AXP < G3.5-COOH. In agreement with the mixed calorimetric responses of G3.5-COOH (exothermic and then endothermic), the molar heat of sorption reaction 1 and sorption reaction 2 (ΔH_{sorp1} = -13 kJ/mol and ΔH_{sorp2} = +22.4 kJ/mol) and associated calculated increasing entropy at equilibrium conditions (ΔS_{sorp1}= -45.4 J/mol K and ΔS_{sorp2} = + 76.0 J/mol K) point to G3.5-COOH shifting

from a more ordered enthalpy-driven association with the surface in the first sorption step towards an entropy-driven sorption type reaction in the second sorption step to allow more adsorption on the surface. This second step entropy-driven sorption is consistent with the PAMAM dendrimers' reported electrostatic intramolecular attraction between their deprotonated carboxylic (COO^-) and protonated tertiary amines (NH_2^+) in their zwitterionic form [54] plausibly causing rearrangement at the ferrihydrite-water interface.

All endothermic ΔH_{desorp} values obtained across reactions pointed to the desorption of G3.5-COOH, AXP, and Pi from ferrihydrite by NO_3^- being an energy consuming, entropy-driven process. Desorption for G3.5-COOH consumed 1-8 times the energy in desorption than sorption. This desorption occurred spontaneously in an environment that involves an entropic shift/increased disorder of 1.5-30 times that of the interface during the sorption steps. It appears that energy shifts associated with reaction step 1 of the sorption and desorption dictated reversibility of G3.5-COOH to ferrihydrite. Despite its significant magnitudinal differences in ΔH_{sorp} and ΔH_{desorp} , all the sorbed G3.5-COOH was desorbed in the desorption phase, with $\Delta H_{desorp}/\Delta H_{sorp}$ and associated entropic shift of 1 and 2 respectively. This indicates that the unit energy involved in the bond forming was equal to that consumed in bond breaking with the ferrihydrite surface, and this was facilitated in an environment where disorder increased by a factor of 2 compared to the sorption state. Contrastingly, for AXP with 86 % reversibility observed, $\Delta H_{desorp}/\Delta H_{sorp}$ and entropic shift between sorption-desorption was 0.5 and 1.5, respectively, pointing to significantly lower energy demand and reorganization of the ferrihydrite-water interface to facilitate its partial desorption.

The comparable nature of molar heats for Pi desorption in reaction 1 and reaction 2 ($\Delta H_{desorp\ 1}$= +21.1 Kj/mol and $\Delta H_{desorp2}$ = +18.8 kJ/mol) to the molar heat of Pi sorption reaction

(ΔH_{sorp} = -25.5 kJ/mol) is reason to postulate that Pi molecules bound to ferrihydrite in a ligand exchange-type reaction were desorbed in these two Pi desorption reactions with entropic swings of 1.85 (Pi desorption 1) and 1.74 (Pi desorption 2) facilitating these desorption reactions. In contrast, with a comparatively weaker ΔH_{desorp} of 9.9 kJ/mol by 0.38-0.52 times the above mentioned ΔH of Pi sorption and desorption reactions, Pi desorption in reaction 3 was most likely associated to previously bound molecules in a strong ion exchange (<10 kJ/mol) type association with ferrihydrite. The absence of a step equivalent to this third Pi desorption step in sorption and the fact that ≈ 7 times more Pi was desorbed compared to Pi previously sorbed indicates that NO_3^- desorption of AXP from the surface mediated hydrolysis which produced more Pi that was subsequently sorbed in a short-range ion exchange type reaction then desorbed by NO_3^-. As shown in Fig. 4-6, the desorption reaction was stopped after ≈ 2.5 hours where effluent concentrations of AXP were non-existent, but residual Pi was still being detected ([Pi] = 0.012 mM) indicating that missing AXP (14%) could still be on the surface being hydrolyzed. It is also plausible that residual Pi being detected after 2.5 hours was previously sorbed Pi being desorbed.

Table 4 - 3 Measured and calculated total energy, quantity, molar heat of reaction, and entropy for sorption reactions of organic acids onto/from ferrihydrite

	G3.5-COOH			ATP		
	Overall	Reaction 1	Reaction 2	Overall	Reaction 1 (AXP)	Reaction 2 (Pi)
Total Energy, Etotal (J/g)	0.162	-0.740	0.902	-8.50	-6.17	-2.33
Quantity (μmol/g)	1.9	1.1	0.8		17870	92
Molar heat of reaction, ΔH (kJ/mol COO^- or $H_2PO_3^-$)	1.7	-13.4	22.4		-0.35	-25.33
Entropy, ΔS (J/mol/K)	5.74	-45.43	75.95		-1.17	-85.81

Table 4 - 4 Measured and calculated total energy, quantity, molar heat of reaction, and entropy for desorption reactions of organic acids onto/from ferrihydrite.

	G3.5-COOH			ATP				
	Overall	Reaction 1	Reaction 2	Overall	Reaction 1 (AXP)	Reaction 2 (Pi)	Reaction 3 (Pi)	Reaction 4 (Pi)
Total Energy, Etotal (J/g)	1.350	1.344		11.63	2.47	3.50	1.35	4.31
Quantity (μmol/g)	1.9	1.9			14650	161	72	435
Molar heat of reaction, ΔH (kJ/mol COO^- or $H_2PO_3^-$)	14.1	14.1			0.17	21.72	18.84	9.90
Entropy, ΔS (J/mol/K)	47.84	47.65			0.57	73.59	63.83	33.54

Effects on ferrihydrite surface charge

Fig. 4-7 shows thermograms for the pre and post amino-bearing organic acids treatment on ferrihydrite anion exchange, NO_3^-/Cl^- and Cl^-/NO_3^-. Comparison between anion exchange thermograms across organic acids indicated that sorption then desorption of G3.5-COOH resulted in increased E_{total} by a factor of 3 for post NO_3^-/Cl^- and Cl^-/NO_3^- exchanges on ferrihydrite while sorption then desorption of ATP resulted in decreased E_{total} by a factor of 2 for NO_3^-/Cl^- and Cl^-/NO_3^- exchanges on ferrihydrite. The increased and decreased E_{total} for anion exchanges on ferrihydrite by G3.5-COOH and ATP respectively, reflect the differences in these molecules' sorption and desorption mechanisms. G3.5-COOH formed completely reversible mixed mixed van der Waals and ion exchange type associations with a NO_3^- saturated ferrihydrite. Then its complete desorption resulted in increased E_{total} for anion exchange through surface-corrosion that left behind more active sites for anion exchange. In contrast, Pi's inner sphere ligand exchange complexation with the surface and the missing AXP (14 %) bound on the surface via the phosphate groups [69] most likely resulted in inner sphere irreversible metal-phosphate complexes [76] with molecules irreversibly bound on anion exchange sites. This is in agreement with the consistent low anion exchange occurring after ATP sorption and desorption with the loss of anion exchange sites found to be irreversible after two cycles of NO_3^-/Cl^- and Cl^-/NO_3^- on the surface.

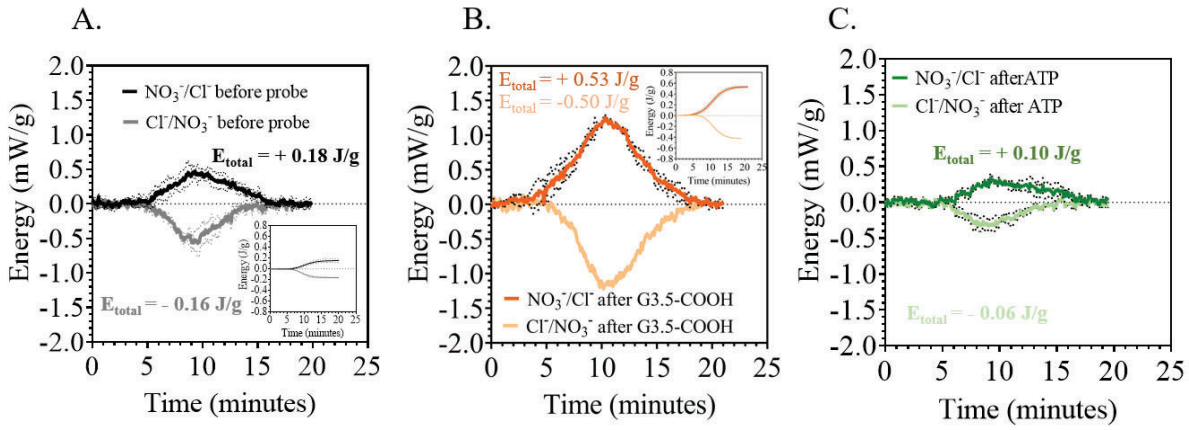

Figure 4-7: Anion exchange energy on ferrihydrite A: before organic acids treatment on ferrihydrite, B: after G3.5-COOH treatment on ferrihydrite, C: after ATP treatment on ferrihydrite

CHAPTER 5: SUMMARY AND CONCLUSIONS

The main objective of this work was to shed light on sorption/desorption dynamics, kinetics, and heat of reaction of different classes of amino-bearing organic acids at the ferrihydrite-water interface. Effects on ferrihydrite surface charge from OM-ferrihydrite associations were also quantified by comparing anion exchange characteristics of the surface determined before sorption reactions and anion exchange characteristics of the surface measured after desorption reactions of previously sorbed organic acids. For this purpose, in-tandem Flow adsorption microcalorimetry– UV-Vis spectroscopy was used to collect the heat and quantities associated with amino-bearing organic acid reactions at the ferrihydrite-water interface. Calorimetric methodologies for probing surfaces and their properties were applied to the adsorption/desorption reactions of a suite of naturally occurring proteinogenic and non-proteinogenic amino acids (glycine, α-alanine, and β-alanine), a bigger, more sturdy, synthetic poly amidoamine dendrimer G3.5-COOH, and a hydrolyzable naturally occurring adenosine triphosphate (ATP).

In Chapters 2 and 3, reactions were conducted at pH 5 where ferrihydrite is predominantly positively charged and glycine, α-alanine, G3.5-COOH, and β-alanine are predominantly in their zwitterionic form. All molecules exhibited a two-step sorption reaction consistent with decreasing rate constant values, *k'*, from step 1 to step 2 towards equilibrium and surface saturation. The exothermic nature of this reaction 1 ($-\Delta H$) was consistent with a well-ordered ferrihydrite interface facilitating enthalpy-driven ion exchange bond formation (Fig. 5-1 A,B,C,D). Towards equilibrium, subsequent sorption resulted in increased disorder in the sequence β-alanine < α-alanine < G3.5-COOH and decreased disorder in glycine which mediated entropic-driven sorption (ΔH values shifting to more positive values) in molecules more prone to

intramolecular interactions (G3.5-COOH) and steric interferences (α-alanine) (Fig. 5-1 A,B,C,D). *ΔH* for the desorption phase pointed to desorption being entropy-driven with molecules that experienced no increase in disorder during the sorption phase (glycine) being completely reversible in a two-step simple ion exchange reaction, while those on a highly disordered ferrihydrite interface required a combination of van der Waals bonding with ion exchange (< 2 kJ/mol) and a stronger ion exchange-type reaction (<10 kJ/mol) to facilitate complete reversibility for G3.5-COOH and β-alanine, and partial reversibility for α-alanine (Fig. 5-2 A,B,C,D).

Chapter 4 presented a side by side analysis of sorption and desorption characteristics of an uncharged hydrolysable ATP and zwitterionic non-hydrolysable G3.5-COOH at the ferrihydrite-water interface. Enthalpy-driven ATP weak van der Waals forces-type association with the surface via its phosphate groups mediated hydrolysis and subsequent resorption of produced inorganic phosphorous by an enthalpy-driven ligand exchange reaction. The exothermic nature of the desorption phase was consistent with increasing entropy on the surface necessary to break the well-ordered and strong bonds (25.3 kJ/mol) between the surface and Pi to facilitate a spontaneous desorption reaction at experimental temperature conditions (22 ^{o}C). Typical of ion exchange associations, the non-hydrolysable G3.5-COOH interactions with ferrihydrite were short (15 minutes) and occurred with *k'* values a magnitude greater than ATP's reactions that were much longer (0.5-2.5 hours).

A comparison between pre-probe and post-probe anion exchange characteristics revealed the effect of sorption then desorption of the different classes of amino-bearing organic acids on the surface charge of ferrihydrite. Zwitterionic molecules whose associations with ferrihydrite are completely reversible in an ion-exchange desorption reaction by NO_3^- (glycine, G3.5-COOH,

and β-alanine) increased E_{total} for anion exchange by corrosion of the surface leaving behind net positive sites (oxygen vacancies) where anion exchange can take place. Zwitterionic molecules irreversibly bound to the surface via an ion exchange-type mechanism (α-alanine) resulted in no effect/slight decrease in E_{total} for anion exchange on the surface. Lastly, ATP generated inorganic phosphorous that sorbed onto ferrihydrite by ligand exchange resulting in inner sphere irreversible metal-phosphate complexes onto sites previously used for anion exchange, thus decreasing E_{total} for the post ATP anion exchange on the surface.

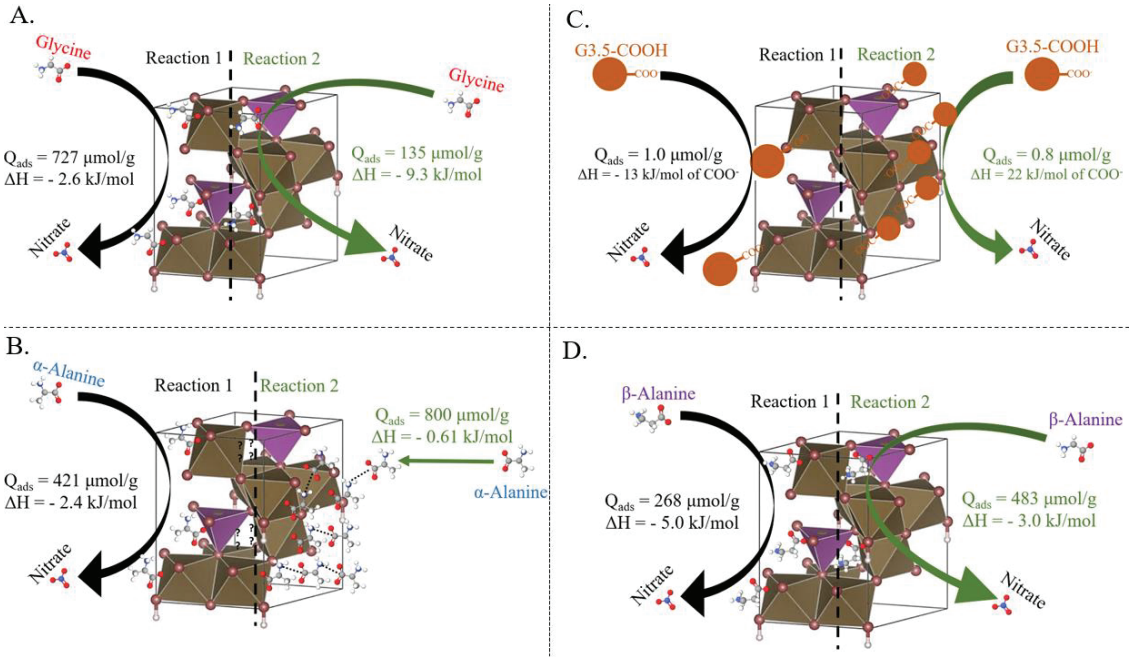

Figure 5-1: Amino-bearing organic acids sorption onto a NO_3^- saturated ferrihydrite. (A): glycine, (B): α-alanine, (C) G3.5-COOH, (D): β-alanine. Filled black arrow: reaction 1 of the sorption stage; Filled green arrow: reaction 2 of the sorption stage. Q_{ads}: quantity sorbed, ΔH: heat of reaction.

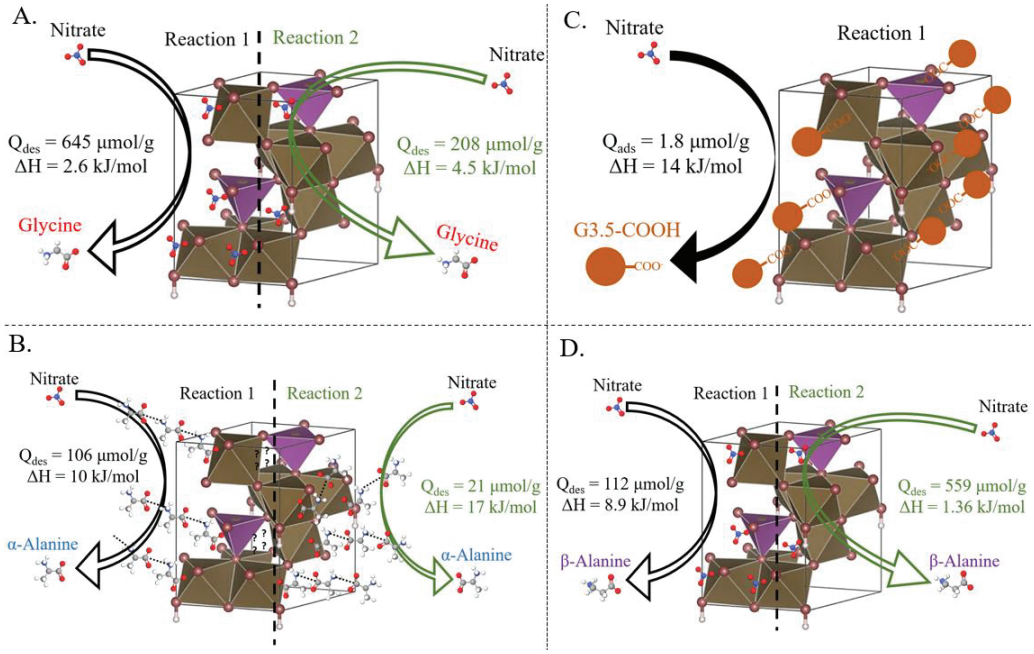

Figure 5-2: Amino-bearing desorption from ferrihydrite by exchange reactions with NO_3^-. (A): glycine, (B): α-alanine, (C): G3.5-COOH, (D) β-alanine. Open black arrow: reaction 1 of the desorption stage, Open green arrow: reaction 2 of the desorption stage, Q_{des}: quantity desorbed, ΔH: heat of reaction.

REFERENCES

1. Wang, S., Xu, J., Zhang, X., Wang, Y., Fan, J., Liu, L., Wang, N., & Chen, D., Structural characteristics of humic-like acid from microbial utilization of lignin involving different mineral types. *Environmental Science and Pollution Research,* **2019,** *26* (23), 23923–23936.
2. Harvey, O. R., Leonce, B. C., & Herbert, B. E., A Flow Adsorption Microcalorimetry-Logistic Modeling Approach for Assessing Heterogeneity of Brønsted-Type Surfaces: Application to Pyrogenic Organic Materials. *Environmental science & technology* **2018,** *52*, 6167-6176.
3. Newcomb, C. J., Qafoku, N. P., Grate, J. W., Bailey, V. L., & de Yoreo, J. J., Developing a molecular picture of soil organic matter–mineral interactions by quantifying organo–mineral binding. *Nature Communications* **2017,** *8* (1).
4. Strawn, D. G., Sorption Mechanisms of Chemicals in Soils. *Soil Systems* **2021,** *5* (1), 13.
5. Kleber, M., Bourg, I. C., Coward, E. K., Hansel, C. M., Myneni, S. C. B., & Nunan, N., Dynamic interactions at the mineral–organic matter interface 2(6), 402–421. *Nature Reviews Earth & Environment* **2021,** *2* (26), 402–421.
6. Pérez-Guzmán, L., Bogner, K. R., Lower, B. H., Earth's Ferrous Wheel. *Nature Education Knowledge* **2010,** *3* (10), 32.
7. Mcbride, M. B., Reactivity of adsorbed and structural iron in hectorite as indicated by oxidation of benzidine. *Clays an d Clay Minerals* **1979,** *27* (3), 224-230.
8. Oades, J. M., The retention of organic matter in soils. *Biogeochemistry* **1988,** *5* (1), 35-70.
9. Parton, W. J., Schimel, D. S., Cole, C. V., & Ojima, D. S., Analysis of Factors Controlling Soil Organic Matter Levels in Great Plains Grasslands. *Soil Science Society of America Journal* **1987,** *51* (5), 1173-1179.
10. Keil, R., & Mayer, L., Mineral matrices and organic matter. *Treatise on Geochemistry* **2014**, 337-359.
11. Brown, G. E., Henrich, V. E., Casey, W. H., Clark, D. L., Eggleston, C., Felmy, A., Goodman, D. W., Grätzel, M., Maciel, G., McCarthy, M. I., Nealson, K. H., Sverjensky, D. A., Toney, M. F., & Zachara, J. M., Metal Oxide Surfaces and Their Interactions with Aqueous Solutions and Microbial Organisms. *Chemical Reviews* **1998,** *99* (1), 77–174.
12. Sollins, P., Peter Homann, and Bruce A Caldwell, Stabilization and destabilization of soil organic matter: mechanisms and controls. *Geoderma* **1996,** *74*, 65-105.
13. Weiler, R., & Mills, A., Surface properties and pore structure of marine sediments. *Deep sea research and Oceanographic Abstracts* **1965,** *12* (4), 511-529.
14. Schimel, D. S., Braswell, B. H., Holland, E. A., McKeown, R., Ojima, D. S., Painter, T. H., Parton, W. J., & Townsend, A. R., Climatic, edaphic, and biotic controls over storage and turnover of carbon in soils. *Global biogeochemical cycles* **1994,** *8* (3), 279-293.
15. (Ed.), I. P. O. C. C., Evaluation of climate models. *Climate change 2013: The Physical Science Basis* **2013**, 741-866.
16. Sposito, P. E. E. E. G., & Sposito, E. O. E. E. G., The Surface Chemistry of Soils. *Oxford University Press*, 1984.
17. Kleber, M., Sollins, P., & Sutton, R., A conceptual model of organo-mineral interactions in soils: self-assembly of organic molecular fragments into zonal structures on mineral surfaces. *Biogeochemistry* **2007,** *85* (1), 9-24.

18. Kleber, M., Eusterhues, K., Keiluweit, M., Mikutta, C., Mikutta, R., & Nico, P. S., Mineral-organic associations: formation, properties, and relevance in soil environments. *Advances in Agronomy* **2015,** *130*, 1-140.
19. Gu, B., Schmitt, J., Chen, Z., Liang, L., & McCarthy, J. F., Adsorption and desorption of natural organic matter on iron oxide: mechanisms and models. *Environmental Science & Technology* **1994,** *28* (1), 38–46.
20. Abarca-Cabrera, L., Fraga-García, P., & Berensmeier, S., Bio-nano interactions: binding proteins, polysaccharides, lipids and nucleic acids onto magnetic nanoparticles. *Biomaterials Research* **2021,** *25* (1).
21. Leinemann, T., Preusser, S., Mikutta, R., Kalbitz, K., Cerli, C., Höschen, C., Mueller, C., Kandeler, E., & Guggenberger, G., Multiple exchange processes on mineral surfaces control the transport of dissolved organic matter through soil profiles. *Soil biology & biochemistry.* **2018,** *118*, 79-90.
22. Evans, L. T. a. R., E.W., The adsorption of humic and fulvic acids by clays. *Journal of soil science* **1959,** *10*, 119-132.
23. Inoue, K., Zhao, L.P. and Huang, P.M., Adsorption of humic substances by hydroxyaluminum-and hydroxyaluminumsilicate-montmorillonite complexes. *Soil science society of America journal* **1990,** *54*, 1166-1172.
24. Schulthess, C. P. a. H., C.P., Humic and fulvic acid adsorption by silicon and aluminum oxide surfaces on clay minerals. *Soil science societty of America journal* **1991,** *55*, 34-42.
25. Tipping, E., The adsorption of aquatic humic substances by iron oxides. *Gecochim. Cosmochim. Acta* **1981,** *45*, 191-199.
26. Helmy, A., Ferreiro, E., & de Bussetti, S., Energy, enthalpy, and isosteric heat of adsorption of phosphate on hydrous Al oxide. *Journal of Colloid and Interface Science* **1996,** *183* (1), 131-134.
27. Weerasooriya, R., Tobschall, H., Wijesekara, H., & Bandara, A., Macroscopic and vibration spectroscopic evidence for specific bonding of arsenate on gibbsite. *Chemosphere* **2004,** *55* (9), 1259-1970.
28. Kaiser, K., & Zech, W., Release of Natural Organic Matter Sorbed to Oxides and a Subsoil. *Soil Science Society of America Journal* **1999,** *63* (5), 1157-1166.
29. Lantenois, S., Prélot, B., Douillard, J. M., Szczodrowski, K., & Charbonnel, M. C., Flow microcalorimetry: Experimental development and application to adsorption of heavy metal cations on silica. *Applied surface science* **2007,** *253* (13), 5807-5813.
30. Swenson, H., and Nicholas P. Stadie, Langmuir's Theory of Adsorption: A Centennial Review. *Langmuir* **2019,** *35* (16), 5409–5426.
31. Harvey, O., & Rhue, R., Kinetics and energetics of phosphate sorption in a multi-component Al(III)–Fe(III) hydr(oxide) sorbent system. *Journal of Colloid and Interface Science* **2008,** *322* (2), 384-393.
32. Schneider, S., Simon, F., Pleul, D., & Jacobasch, H. J., Flow sorption calorimetry, a powerful tool to invesitgate the acid base character of organic polymer surfaces. *Fresenius' Journal of Analytical Chemistry* **1997,** *358* (1-2), 244-247.
33. Taraba, B., Reversible and irreversible interaction of oxygen with coal using pulse flow calorimetry. *Fuel* **1990,** *69* (9), 1191-1199.
34. Meziani, M. J., Zajac, J., Jones, D. J., Rozière, J., & Partyka, S., Surface characterization of mesoporous silicoaluminates of MCM-41 type: evaluation of polar surface sites using flow calorimetry, adsorption of cationic surfactant as a function of pore size and aluminum content. *Langmuir* **1997,** *13* (20), 5409-541.

35. Jojima, T., Vertès, A. A., Inui, M., & Yukawa, H., Development of Growth-Arrested Bioprocesses with Corynebacterium glutamicum for Cellulosic Ethanol Production from Complex Sugar Mixtures. *Biorefineries* **2014**, 121-139.
36. Parthasarathy, A., Savka, M. A., & Hudson, A. O., The Synthesis and Role of β-Alanine in Plants. *Frontiers in Plant Science* **2019,** *10*.
37. Crea, F., de Stefano, C., Gianguzza, A., Piazzese, D., & Sammartano, S., Chemical speciation of organic matter in natural waters. Interaction of nucleotide 5' mono-, di- and triphosphates with major components of seawater. *Chemical Speciation and Bioavailability* **2004,** *16* (1-2), 1-8.
38. Li, Q., Snoeyink, V. L., Mariãas, B. J., & Campos, C., Elucidating competitive adsorption mechanisms of atrazine and NOM using model compounds. *Water Research* **2003,** *37* (4), 773-784.
39. Klein, A. R., Bone, S. E., Bakker, E., Chang, Z., & Aristilde, L., Abiotic phosphorus recycling from adsorbed ribonucleotides on a ferrihydrite-type mineral: Probing solution and surface species. *Journal of Colloid and Interface Science* **2019,** *547*, 171-182.
40. Doucette, W. J., Quantitative structure–activity relationships for predicting soil–sediment sorption coefficients for organic chemicals. *Environmental Toxicology and Chemistry* **2003,** *22* (8), 1771.
41. Greathouse, J., Johnson, K., & Greenwell, H., Interaction of Natural Organic Matter with Layered Minerals: Recent Developments in Computational Methods at the Nanoscale. *Minerals* **2014,** *4* (2), 519–540.
42. Abarca-Cabrera, L., Fraga-García, P., & Berensmeier, S., Bio-nano interactions: binding proteins, polysaccharides, lipids and nucleic acids onto magnetic nanoparticles. *Biomaterials Research* **2021,** *25* (1).
43. Oren, A., & Chefetz, B., Sorptive and Desorptive Fractionation of Dissolved Organic Matter by Mineral Soil Matrices. *Journal of Environmental Quality* **2012,** *41* (2), 526–533.
44. Gu, B., Schmitt, J., Chen, Z., Liang, L., & McCarthy, J. F., Adsorption and desorption of natural organic matter on iron oxide: mechanisms and models. *Environmental Science & Technology* **1994,** *28*, 38–46.
45. Leinemann, T., Preusser, S., Mikutta, R., Kalbitz, K., Cerli, C., Höschen, C., Mueller, C., Kandeler, E., & Guggenberger, G., Multiple exchange processes on mineral surfaces control the transport of dissolved organic matter through soil profiles. *Soil Biology and Biochemistry* **2018,** *118*, 79-90.
46. Kabengi, N. J., Rhue, R. D., & Daroub, S. H., Using flow calorimetry to determine the molar heats of cation and anion exchange and the point of zero net charge on amorphous aluminum hydroxides. *Soil science* **2006,** *171* (1), 13-20.
47. Villacís García, M., Ugalde Arzate, M., Vaca Escobar, K., Villalobos, M., Zanella, R., & Martínez Villegas, N., Laboratory Synthesis of Goethite and Ferrihydrite of Controlled Particle Sizes. *Boletín de la Sociedad Geológica Mexicana* **2015,** *67* (3), 433-446.
48. Hanczyc, M. M., Mansy, S. S., & Szostak, J. W. (2006). Mineral Surface Directed Membrane Assembly, Mineral Surface Directed Membrane Assembly. *Origins of Life and Evolution of Biospheres* **2006,** *37* (1), 67-82.
49. Corporation, R. A., Rigaku Global Website. *Rigaku* **2022**.
50. instruments, T., TA Instruments. *TA Instruments* **2022**.
51. Allen, N., Machesky, M. L., Wesolowski, D. J., & Kabengi, N., Calorimetric study of alkali and alkaline-earth cation adsorption and exchange at the quartz-solution interface. *Journal of Colloid and Interface Science* **2017,** *504*, 538-548.

52. Burke C. Leonce, W. C. H., Manyiel M. Mel, Aurore Niyitanga Manzi, Omar Harvey, Sorption dynamics and energatics of cinnamic acid and its derivatives at the ferrihydrite-water interface determined by flow-adsorption microcalorimetry *American chemical society* **2022**.
53. Hiemstra, T., Formation, stability, and solubility of metal oxide nanoparticles: Surface entropy, enthalpy, and free energy of ferrihydrite. *Geochimica et Cosmochimica Acta* **2015,** *158*, 179–198.
54. Geitner, N. K., Wang, B., Andorfer, R. E., Ladner, D. A., Ke, P. C., & Ding, F., Structure–Function Relationship of PAMAM Dendrimers as Robust Oil Dispersants. *Environmental Science & Technology* **2014,** *48* (21), 12868–12875.
55. Hashizume, H., Adsorption of DL-alanine by Allophane: Effect of pH and Unit Particle Aggregation. *Clay Minerals* **1999,** *34* (2), 233–238.
56. Garcia, A. R., Brito De Barros, R., Fidalgo, A., & Ilharco, L. M., Interactions of l-Alanine with Alumina as Studied by Vibrational Spectroscopy. *Langmuir* **2007,** *23*, 10164-10175.
57. Polisi, M., Fabbiani, M., Vezzalini, G., di Renzo, F., Pastero, L., Quartieri, S., & Arletti, R., Amino acid encapsulation in zeolite MOR: Effect of spatial confinement. . *Physical Chemistry Chemical Physics* **2021,** *23* (36), 20541–20552.
58. Merola, C., Cheng, H. W., Schwenzfeier, K., Kristiansen, K., Chen, Y. J., Dobbs, H. A., Israelachvili, J. N., & Valtiner, M., In situ nano- to microscopic imaging and growth mechanism of electrochemical dissolution (e.g., corrosion) of a confined metal surface. *Proceedings of the National Academy of Sciences* **2017,** *114* (36), 9541–9546.
59. Yu, X. X., Han, J., Scully, J. R., & Marks, L. D., Oxygen injection during fast vs slow passivation in aqueous solution. *Acta Materialia* **2021,** *213*.
60. Noam, L., Minerals and the origin of life: hypotheses and experiments in heterogeneous chemistry. *Heterogeneous Chemistry Reviews* **1994,** *1* (2), 159-179.
61. Weids, A. J., Ibstedt, S., Tamás, M. J., & Grant, C. M., Distinct stress conditions result in aggregation of proteins with similar properties. *Scientific Reports* **2016,** *6* (1).
62. Madine, J., Wang, X., Brown, D. R., & Middleton, D. A., Evaluation of β-Alanine- and GABA-Substituted Peptides as Inhibitors of Disease-Linked Protein Aggregation. *ChemBioChem* **2009,** *10* (12), 1982–1987.
63. Madine, J., Doig, A. J., & Middleton, D. A., Design of an N-Methylated Peptide Inhibitor of α-Synuclein Aggregation Guided by Solid-State NMR. . *Journal of the American Chemical Society* **2008,** *130* (25), 7873–7881.
64. Sciarretta, K. L., Gordon, D. J., & Meredith, S. C., Peptide-Based Inhibitors of Amyloid Assembly. *Amyloid, Prions, and Other Protein Aggregates* **2006,** *Part C*, 273–312.
65. Olsson, R., Giesler, R., Loring, J. S., & Persson, P., Enzymatic Hydrolysis of Organic Phosphates Adsorbed on Mineral Surfaces. *Environmental Science & Technology,* **2011,** *46* (1), 285–291.
66. Hayes, J. E., Richardson, A. E., & Simpson, R. J., Components of organic phosphorus in soil extracts that are hydrolysed by phytase and acid phosphatase. *Biology and Fertility of Soils* **2000,** *32* (4), 279–286.
67. Shand, C. A., & Smith, S., Enzymatic release of phosphate from model substrates and P compounds in soil solution from a peaty podzol. *Biology and Fertility of Soils,* **1997,** *24* (2), 183–187.
68. Sun, M., Alikhani, J., Massoudieh, A., Greiner, R., & Jaisi, D. P., Phytate Degradation by Different Phosphohydrolase Enzymes: Contrasting Kinetics, Decay Rates, Pathways, and Isotope Effects. *Soil Science Society of America Journal,* **2017,** *81* (1)), 61–75.

69. Klein, A. R., Bone, S. E., Bakker, E., Chang, Z., & Aristilde, L., Abiotic phosphorus recycling from adsorbed ribonucleotides on a ferrihydrite-type mineral: Probing solution and surface species. *Journal of Colloid and Interface Science* **2019,** *547*, 171–182.
70. Levy-Booth, D. J., Campbell, R. G., Gulden, R. H., Hart, M. M., Powell, J. R., Klironomos, J. N., Pauls, K. P., Swanton, C. J., Trevors, J. T., & Dunfield, K. E. , Cycling of extracellular DNA in the soil environment. . *Soil Biology and Biochemistry* **2007,** *39* (12), 2977–2991.
71. Pietramellara, G., Ascher, J., Borgogni, F., Ceccherini, M. T., Guerri, G., & Nannipieri, P., Extracellular DNA in soil and sediment: fate and ecological relevance. *Biology and Fertility of Soils,* **2008,** *45* (3).
72. Bhattacharyya, A., Campbell, A. N., Tfaily, M. M., Lin, Y., Kukkadapu, R. K., Silver, W. L., Nico, P. S., & Pett-Ridge, J. x., Redox Fluctuations Control the Coupled Cycling of Iron and Carbon in Tropical Forest Soils. *Environmental Science & Technology* **2018** *52* (24), 14129–14139.
73. Herndon, E. M., Kinsman-Costello, L., Duroe, K. A., Mills, J., Kane, E. S., Sebestyen, S. D., Thompson, A. A., & Wullschleger, S. D., Iron (Oxyhydr)Oxides Serve as Phosphate Traps in Tundra and Boreal Peat Soils. . *Journal of Geophysical Research: Biogeosciences* **2019,** *124* (2), 227–246.
74. Eaton, A. D. C. L. S. R. E. W. G. A. E. F. M. H., Eds., Standard Methods for the Examination of Water and Wastewater. *American Public Health Association: Washington, DC, Water Environment Federation: Alexandria, VA, and American Water Works association: Denver, CO* **2005**.
75. Kwon, K. D., & Kubicki, J. D., Molecular Orbital Theory Study on Surface Complex Structures of Phosphates to Iron Hydroxides: Calculation of Vibrational Frequencies and Adsorption Energies. *Languimir* **2004,** *20* (21), 9249-9254.
76. Persson, P., Nilsson, N., & Sjöberg, S., Structure and Bonding of Orthophosphate Ions at the Iron Oxide–Aqueous Interface. Journal of Colloid and Interface Science. *177* **1996,** (1), 263–275.
77. Gurtler, J., & Mai, T., Traditional preservatives-Organic acids. *Encyclopedia of Food Microbiology* **2014**, 119-130.
78. Dyer, J. A., Trivedi, P., Scrivner, N. C., & Sparks, D. L., Lead Sorption onto Ferrihydrite. 2. Surface Complexation Modeling. *Environmental Science & Technology* **2003,** *37* (5), 915–922.
79. Schwertmann, U., Fechter, H., The point of zero charge of natural and synthetic ferrihydrites and its relation to adsorbed silicate. *Clay Minerals* **1982,** *17*, 471-476.

APPENDIX

Properties of ferrihydrite

The formation of 2-line ferrihydrite was confirmed by x-ray diffraction analysis that displayed the presence of two [77] bands centered at 2θ of 34° and 61° (Fig. A 1). The absence of narrow sharp peaks in the XRD pattern of ferrihydrite indicated that it is highly amorphous. The thermal analysis of ferrihydrite confirmed the amorphous nature of ferrihydrite by exhibiting free-water loss in two stages (40 – 140 °C), followed by structural-water (140 – 320 °C), and chemical water loss at higher temperatures (320 – 400 °C) (Fig. A 2). Scanning Electron Microscopy [48] showed that ferrihydrite grains used in experiments (size 125-250 μm) were aggregated (Fig. A 3) with a median diameter (D_{50}) of 158 ± 10 μm (Fig. A 4). With its well documented and published point of zero charge (PZC pH 7- 9) [78, 79], at pH 5 ferrihydrite had 99 - 99.99% of its positive sites (M-OH_2^+, where M is Fe) (Fig. A 5).

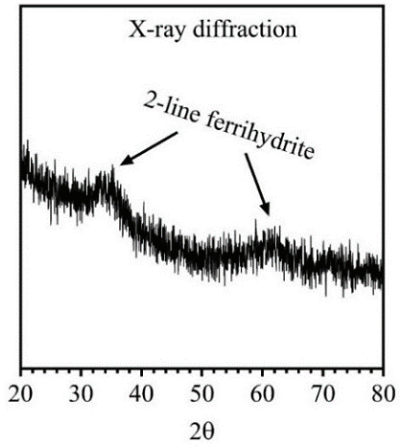

Figure A 1: X-ray diffractogram of ferrihydrite with characteristic 2θ peaks for the two-line form around 34° and 61°.

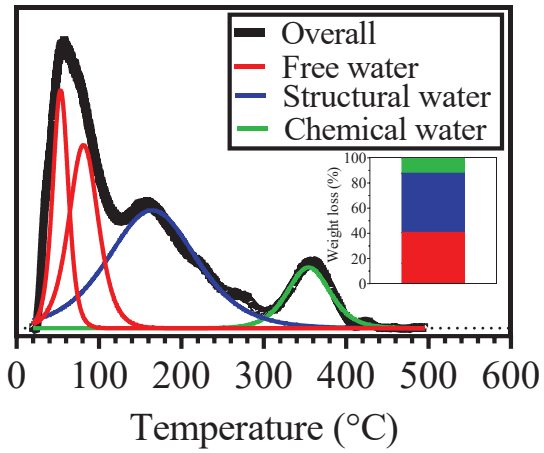

Figure A 2: Differential thermogravimetric thermogram showing deconvoluted proportions of free (red lines), structural (blue line) and chemical (green line) water associated with the 2-line ferrihydrite (inset).

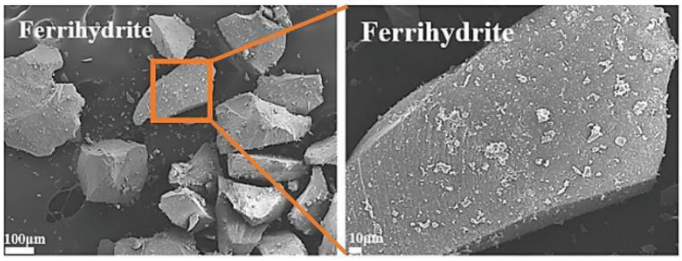

Figure A 3: An example of a scanning electron microscope image for the 125-250 µm ferrihydrite fraction showing irregularly shaped morphology.

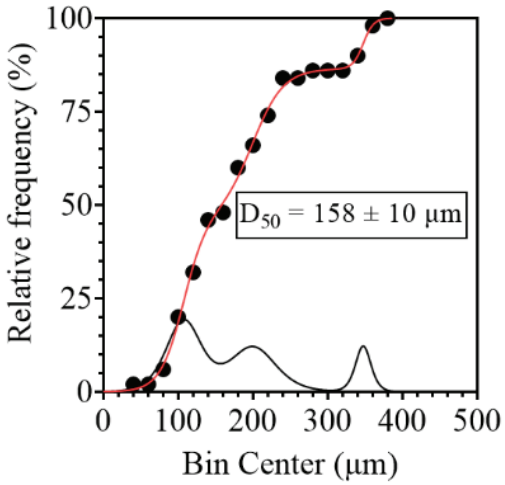

Figure A 4: Particle size distribution for the 125-250 µm ferrihydrite fraction derived from Image J analysis of 50 randomly selected particles in scanning electron microscope.

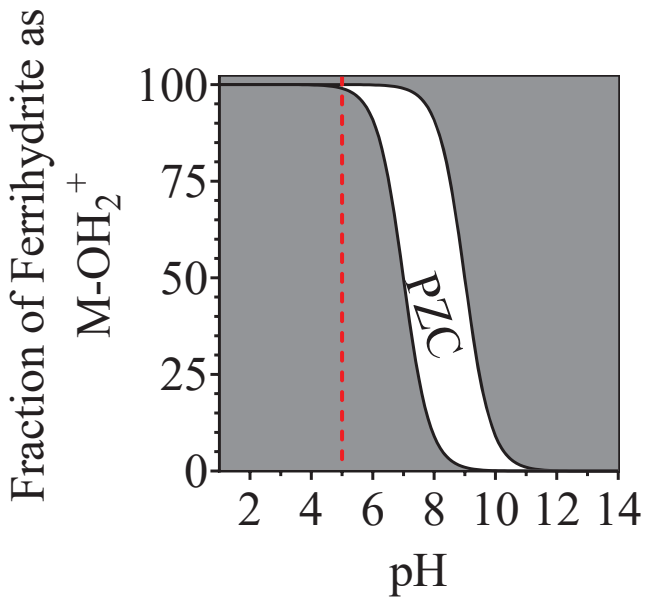

Figure A 5: Modeled distribution of positive charge (M-OH_2+) on ferrihydrite across pH based on published point of zero charge (PZC) values.

Speciation of amino-bearing organic acids

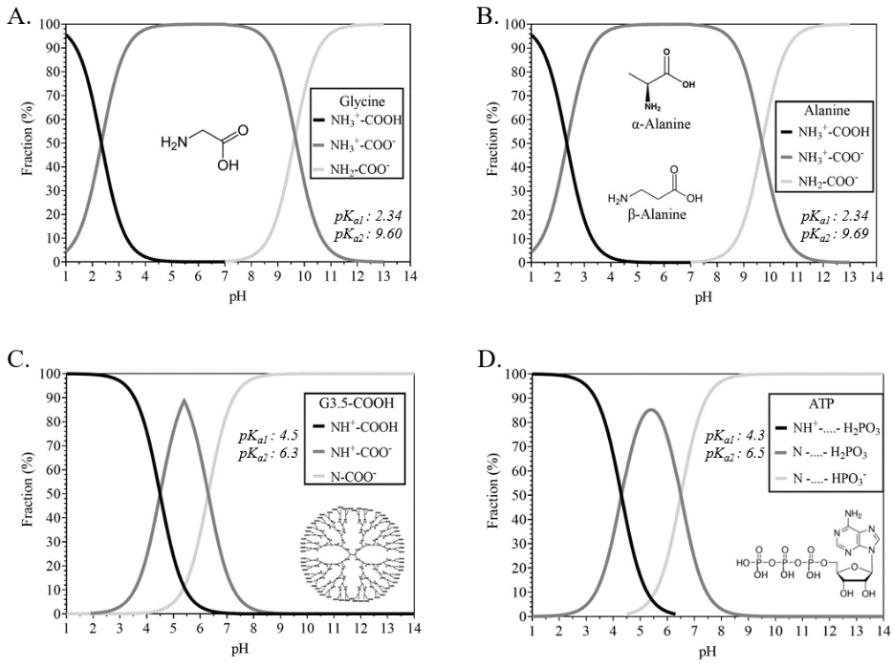

Figure A 6. Predominant forms of selected amino-bearing organic acids: cation at pH < pKa1, zwitterion at pKa1 < pH < pKa2, and anion at pH > pKa2 for (A) glycine, (B) alanine, (C) Poly amido amine (PAMAM) dendrimer G3.5-COOH. Cation at pH < pKa1, neutral at pKa1 < pH < pKa2, and anion at pH > pKa2 for (D) Adenosine triphosphate. Graphs developed using the Henderson-Hasselbalch equation and the published pK_{as} of respective molecules.

Data handling and processing protocol for FAMC-UV-vis

Raw heat flow thermograms were integrated to obtain the area under the peaks and then the energy (J) associated with each heat thermogram was interpolated from the standard curve shown in Fig. A 7. Weight-adjusted energy (E_i; J/g) associated with thermograms was obtained by normalizing the obtained energy (J) to the mass of ferrihydrite used in the experiments (50 ± 0.05 mg).

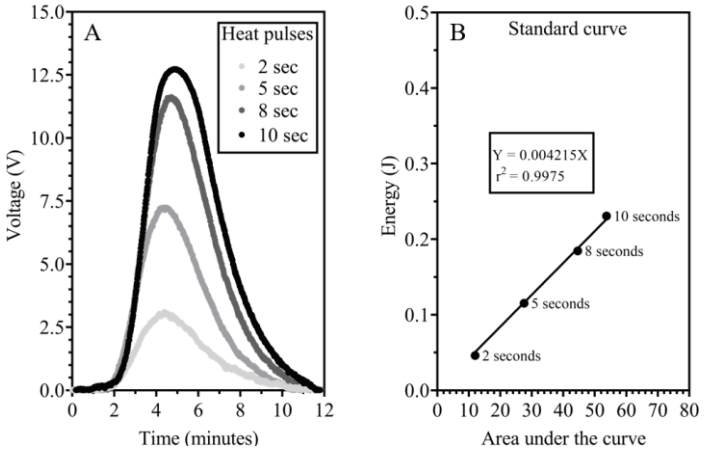

Figure A 7. Peaks obtained from timed heat pulses (A) and the associated calibration curve (B).

Deconvolution of E_i (J/g) was used to assess the number of reaction steps, their respective contribution to total reaction, and respective rate constants. Here equation [2-2] was used and Root Mean Square Error (RMSE) values were used to determine how far apart the predicted values and residuals were from the values in the dataset. Adjusting the logistic model for more reactions/steps allowed for improved RMSE values (Fig. A 8). The best fit model was indicated by minimal change in the RMSE value as more steps were added (Fig. A 8). Apart from the G3.5-COOH desorption reaction that was found to occur in one step, all other reactions for all molecules were found to occur in two steps.

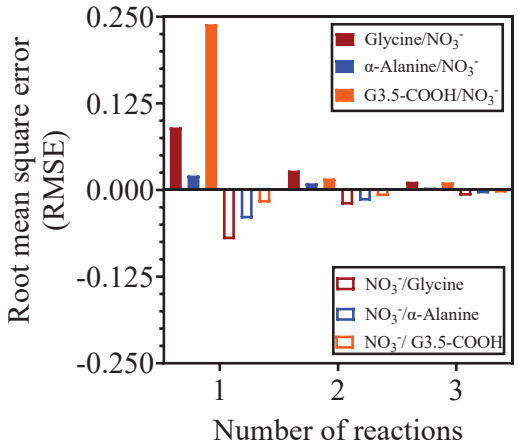

Figure A 8: Root Mean Square Error values associated with the deconvolution of E_i (J/g) energy curves

Raw UV-Vis absorbance data (Fig. A 9) were used to interpolate the amount of each amino-bearing organic acid sorbed (Q_{sorp} ; mmol) and desorbed Q_{desorp}; mmol) onto/from ferrihydrite. Q_{sorp} and desorbed Q_{desorp} were interpolated using previously built standard curves at each molecules' monitoring wavelength (Fig. A 10).

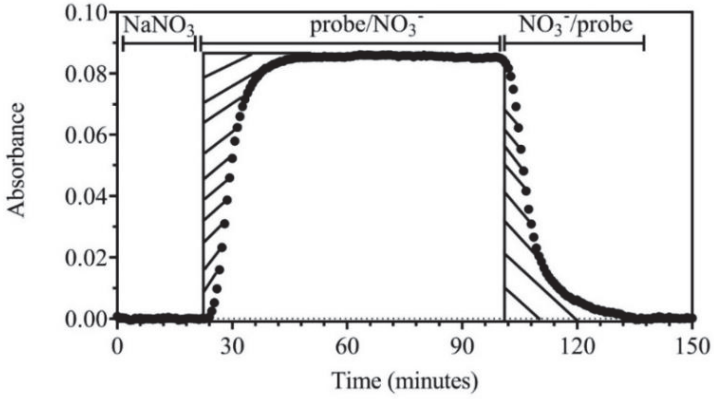

Figure A 9: Analysis of the portion of probe sorbed and desorbed. The points represent the breakthrough curve as the reaction progressed. The shaded area above the breakthrough curve is the portion of the probe bound onto ferrihydrite during the probe/NO_3^- cycle. The shaded area under the breakthrough curve is the portion of previously bound probe removed from ferrihydrite during the NO_3^-/probe cycle.

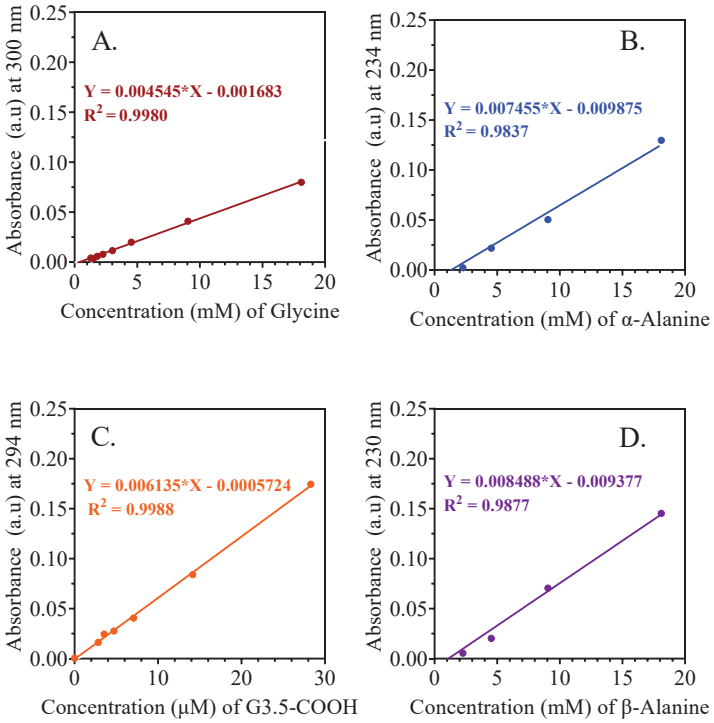

Figure A 10. Standard curves (A: glycine, B: α-alanine, C: G3.5-COOH, D: β-alanine) built at monitoring wavelengths to interpolate concentrations from absorbance.

The obtained quantity (mmol) was then normalized to the mass of ferrihydrite used in the experiments to obtain the sorbed and desorbed quantity in mmol/g. Q_{sorp} (mmol/g) and Q_{desorp} (mmol/g) were then deconvoluted using equation [2-3] and $t_{1/2}$ parameters obtained from deconvoluted energy curves (E_i; J/g) to obtain corresponding quantity data. This was to make sure that energy peaks linked to quantity peaks were synchronous and achieved $t_{1/2}$ at the same time.

The molar heat of reactions in kJ/mol were determined and calculated according to the equation:

$$\Delta H = \frac{E_{total}}{Q_{total}} \qquad [1\text{-}1]$$

VITAE

Personal background	Marie Aurore Niyitanga Manzi Rwanda, Kigali Daughter of Ignace Niyitanga and Odette Mukamanzi
Education	Bachelor of Science, Environmental science, Texas Christian University Fort worth, 2020
Experience	Research assistantship, FROGGS Lab, 2019-present Teaching Assistantship, Texas Christian University 2020-2021
Professional Memberships	American Geophysical Union

ABSTRACT

INTERACTIONS OF AMINO-BEARING ORGANIC ACIDS AT THE FERRIHYDRITE-WATER INTERFACE: A FLOW ADSORPTION MICROCALORIMETRY-ULTRA VIOLET VISIBLE SPECTROSCOPY STUDY

By

Marie Aurore Niyitanga Manzi

Department of Geological sciences

Texas Christian University

Thesis advisor: Dr. Omar Harvey, Department of Geological Sciences

In-tandem flow adsorption microcalorimetry-UV-Vis spectroscopy was used to study the dynamics, kinetics, energetics, and effects on surface charge for amino-bearing organic acids at the ferrihydrite-water interface. The amino-bearing organic acids sorbed to ferrihydrite via multiple, enthalpy- or entropy-driven steps at different rates involving a mixture of van der Waals, ion exchange and ligand exchange reactions. The nature of interaction varied across speciation, molecular size, conformation, and hydrolizability. For instance, glycine sorption to NO_3^--saturated ferrihydrite was a two-step enthalpy-driven, completely reversible ion exchange process with overall heat of sorption (ΔH_{sorp}) of -3.66 kJ mol^{-1} and after the desorption reaction, the anion exchange energy (NO_3^-/Cl^- and Cl^-/NO_3^-) at the ferrihydrite-water interface was doubled. By comparison, α-alanine, with similar speciation as glycine, had two-stepped and enthalpy-driven sorption that occurred via mixed van der Waals and ion exchange reactions with ΔH_{sorp} of -1.24 kJ mol^{-1}, and 10% reversibility by NO_3^- with no impact on anion exchange energy. The thesis further covers comparison in interactions at the ferrihydrite-water interface across molecular conformation (α-alanine versus β-alanine) and hydrolyzability (G3.5-COOH, ATP).